DEPARTMENT OF ELECTRICAL AND COMPUTER ENGINEERING
COLLEGE OF ENGINEERING AND TECHNOLOGY
OLD DOMINION UNIVERSITY
NORFOLK, VIRGINIA 23529

GUIDANCE AND CONTROL STRATEGIES FOR AEROSPACE VEHICLES

By

Desineni S. Naidu, Research Associate

and

Joseph L. Hibey, Principal Investigator

Progress Report
For the period January 1, 1988 to June 30, 1988

Prepared for the
National Aeronautics and Space Administration
Langley Research Center
Hampton, Virginia

Under
Research Grant NAG-1-736
Dr. Douglas B. Price, Technical Monitor
GCD-Spacecraft Control Branch

July 1988

DEPARTMENT OF ELECTRICAL AND COMPUTER ENGINEERING
COLLEGE OF ENGINEERING AND TECHNOLOGY
OLD DOMINION UNIVERSITY
NORFOLK, VIRGINIA 23529

GUIDANCE AND CONTROL STRATEGIES FOR AEROSPACE VEHICLES

By

Desineni S. Naidu, Research Associate

and

Joseph L. Hibey, Principal Investigator

Progress Report
For the period January 1, 1988 to June 30, 1988

Prepared for the
National Aeronautics and Space Administration
Langley Research Center
Hampton, Virginia

Under
Research Grant NAG-1-736
Dr. Douglas B. Price, Technical Monitor
GCD-Spacecraft Control Branch

Submitted by the
Old Dominion University Research Foundation
P. O. Box 6369
Norfolk, VA 23505

July 1988

GUIDANCE AND CONTROL STRATEGIES FOR AEROSPACE VEHICLES

By

Desineni S. Naidu[1] and Joseph L. Hibey[2]

SUMMARY

Enclosed is the List of of Publications/Reports and two reports on the above titled project for the period January 1, 1988 to June 30, 1988.

[1] Research Associate, Department of Electrical and Computer Engineering, Old Dominion University, Norfolk, Virginia 23529

[2] Associate Professor, Department of Electrical and Computer Engineering, Old Dominion University, Norfolk, Virginia 23529

List of Publications/Reports

(i) D. S. Naidu and D. B. Price, "On the method of matched asymptotic expansions", accepted for publication in Journal of Guidance, Control and Dynamics, 1988 (in press).

(ii) D. S. Naidu, "There-dimensional atmospheric entry problem using method of matched asymptotic expansions", 1988 American Control Conference, Atlanta, GA, June 14-17, 1988.

(iii) D. S. Naidu and D. B. Price, "On singular perturbation and time scale approaches in discrete control systems", accepted for publication in Journal of Guidance, Control and Dynamics, 1988 (in press).

(iv) D. S. Naidu and D. B. Price, "Singular perturbations and time scales in digital flight control systems", NASA Technical Paper, Spacecraft Control Branch, Langley Research Center, Hampton (in preparation).

*(v) D. S. Naidu, "Fuel-optimal trajectories for aeroassisted, coplanar, oribital transfer problem", Report, ODU Research Foundation, Norfolk, VA, July, 1988.

*(vi) D. S. Naidu, "Fuel-optimal trajectories for aeroassisted, noncoplanar, orbital transfer problem", Report, ODU Research Foundation, Norfolk, VA, July, 1988.

(vii) D. S. Naidu, J. L. Hibey, and C. Charalambous, "Optimal control of aeroassisted, coplanar, orbital transfer vehicles", Accepted for presentation at 26 IEEE Conference on Decision and Control, Austin, Texas, December 7-9, 1988 [Short version of (vi)].

* copies enclosed

****

FUEL-OPTIMAL TRAJECTORIES FOR AEROASSISTED COPLANAR ORBITAL TRANSFER PROBLEM

Dr. D. S. Naidu
ODU Research Foundation
Norfolk, VA, 23508

ABSTRACT: The optimal control problem arising in coplanar, orbital transfer employing aeroassist technology is addressed. The maneuver involves the transfer from high Earth orbit to low Earth orbit. A performance index is chosen to minimize the fuel consumption for the transfer. Simulations are carried out for establishing a corridor of entry conditions which are suitable for flying the spacecraft through the atmosphere. A highlight of the paper is the application of an efficient multiple shooting method for taming the notorious non-linear, two-point, boundary value problem resulting from optimization procedure.

NOMENCLATURE

A : constant = $S\rho_s/2m$

A_1 : constant = $C_{d0}S\rho_s H_a/2m$

A_2 : constant = $C_{LR}S\rho_s H_a/2m$

a_d : ratio of R_d/R_a

a_c : ratio of R_c/R_a

b : constant = R_a/H_a

C_D : drag coefficient

C_{DO}: zero-lift drag coefficient

C_L : lift coefficient

C_{LR}: lift coefficient for maximum lift-to-drag ratio

c : ratio of C_L/C_{LR}

c : subscript for circularization or reorbit

D : drag force

d : subsript for deorbit

E_m : maximum of (L/D)

g : gravitational acceleration

g_s : gravitational acceleration at surface level

H : altitude

$\mathcal{H}$: Hamiltonian

h : subscript for Hohmann transfer

i : subscript for idealized transfer

J : performance index

K : induced drag factor

L : lift force

m : vehicle mass

R : distance from vehicle center of gravity to Earth center

R_a : radius of the atmospheric boundary

R_c : radius of the low Earth orbit

R_d : radius of the high Earth orbit

R_E : radius of Earth

R_s : distance from vehicle center of gravity to surface level

S : aerodynamic reference area

$_s$: subscript for surface level

t : time

V : velocity

v : normalized velocity

β : inverse atmospheric scale height

γ : flight path angle

δ : normalized density

λ : costate (Langrange) varible

μ : gravitational constant of Earth

ρ : density

τ : normalized time

ΔV : characteristic velocity

Δv : normalized characteristic velocity

1. INTRODUCTION

In space transportation systems, the concept of aeroassisted orbital transfer opens new mission opportunities, especially with regard to the initiation of a permanant space station [1]. The use of aeroassisted maneuvers to affect a transfer from high Earth orbit (HEO) to low Earth orbit (LEO) has been reccommended to provide high performance leverage to future space transportation systems. The space-based orbit transfer vehicle (OTV) is planned as a system for transporting payloads between LEO and other locations in space. The OTV, on its return journey from HEO, dissipates orbital energy through atmospheric drag to slow down to LEO velocity. In a synergetic maneuver for aeroassited orbital transfer vehicles (AOTV's), the basic idea is to employ a hybrid combination of propulsive maneuvers in space and aerodynamic maneuvers in sensible atmosphere [2-4].

In this report, we first describe briefly the various types of coplanar transfers [5]. Then we address the fuel-optimal control problem arising in coplanar orbital transfer employing aeroassist technology. The maneuver involves a transfer from HEO to LEO and at the same time minimization of the fuel consumption for achieving the desired orbit transfer. It is known that a change in velocity, also called the characteristic velocity, is a convenient parameter to measure the fuel consumption. A suitable performance index is the total characteristic velocity which is the sum of the characteristic velocities for deorbit and for reorbit (or circularization) [6]. Use of Pontryagin minimum principle leads to a nonlinear, two-point, boundary value problem (TPBVP) in state and costate variables. This problem is solved by

using an efficient multiple shooting method [7,8]. Simulations are carried out for establishing a spectrum of entry conditions which are suitable for flying the spacecraft through the atmosphere.

2. TYPES OF COPLANAR ORBITAL TRANSFERS

In transferring a vehicle from one orbit, say High Earth Orbit to another orbit, say Low Earth Orbit, in the same plane, we consider the following three types of orbital transfer.

(i) Hohmann transfer
(ii) Idealized aeroassisted transfer
(iii) Realistic aeroassisted transfer

(i) Hohmann Transfer

This is a coplanar transfer in which the vehicle is transferred from HEO to LEO in an all-proplusive manner (Figure 1). The first tangential impulse ΔV_d, called the deorbit impulse, at the radius R_d of HEO, is executed to transfer the vehicle from circular orbit to elliptic orbit with its perigee at R_c. The second tangential impulse ΔV_c, called the circularization or reorbit impulse, at the radius R_c of LEO, is imparted to transfer the elliptic orbit to circular orbit. Thus, the total characteristic velocity ΔV_h, a measure of fuel consumption in achieving the Hohmann transfer, is given by the sum of the deorbit impulse ΔV_d, and the cirularization impulse ΔV_c.

Using the principle of conservation of angular momenutum, the expressions for the deorbit and cirucularization impulses are given by [5]

$$\Delta V_{dh} = \sqrt{\mu/R_d}\left[1 - \sqrt{2/(1+R_d/R_c)}\right] \tag{1}$$

$$\Delta V_{ch} = \sqrt{\mu/R_c}\left[\sqrt{2(R_d/R_c)/(1+R_d/R_c)} - 1\right] \tag{2}$$

Using the normalized values,

$$a_d = R_d/R_a; \quad a_c = R_c/R_a; \quad \Delta v = \Delta V/\sqrt{\mu/R_a} \tag{3}$$

in (1) and (2), we get

$$\Delta v_{dh} = \sqrt{1/a_d} - \sqrt{2a_c/a_d(a_d+a_c)} \tag{4}$$

$$\Delta v_{ch} = \sqrt{2a_d/a_c(a_d+a_c)} - \sqrt{1/a_c} \tag{5}$$

so that the total characteristic velocity in the normalized form is given by

$$\Delta v_h = \Delta v_{dh} + \Delta v_{ch} \tag{6}$$

(ii) Ideal Aeroassisted Transfer

In an idealized aeroassisted coplnar transfer, the vehicle grazes the atmospheric boundary, undergoes the necessary velocity reduction and skips back into another oribit (Figure 2). Thus, the vehicle leaves HEO at R_d with a tangential deorbit impulse ΔV_{di} and enters into an elliptic orbit with its perigee at R_a and flight path angle $\gamma_e = 0$. When the vehicle is at perigee E, its lifting capability (in this case negative lift) is employed to affect flight path along the boundary of the atmosphere (i.e., along the circular orbit of radius R_a). This grazing flight is continued along the atmospheric boundary to point F until sufficient velocity has been depleted by atmospheric drag such that upon reducing the lift to zero, the vehicle ascends with $\gamma_f = 0$ on an elliptic orbit to an apogee at R_c. Finally, at point C, a tangential circularizing burn ΔV_{ci} is imparted to achieve the desired LEO. In this transfer, the idealizations are (i) the atmospheric density at R_a is sufficient to generate enough drag to slow the vehicle in a reasonable amount of time, and (ii) the vehicle has sufficient lifting capability to maintain fligh along the atmospheric boundary.

The following relations for the characteristic velocities are obtained by using the principles of conservation of angular momenutum and the conservation of energy. The deorbit impulse ΔV_{di} given by

$$\Delta V_{di} = \sqrt{\mu/R_d} - \sqrt{2(\mu/R_a)/(R_d/R_a)(R_d/R_a+1)} \tag{7}$$

and the circularization or reorbit impulse ΔV_{ci} turns out to be

$$\Delta V_{ci} = \sqrt{\mu/R_c} - \sqrt{2(\mu/R_a)/(R_c/R_a)(R_c/R_a+1)} \tag{8}$$

In terms of the normalized values (3),

$$\Delta v_{di} = \sqrt{1/a_d} - \sqrt{2/a_d(a_d+1)} \tag{9}$$

$$\Delta v_{ci} = \sqrt{1/a_c} - \sqrt{2/a_c(a_c+1)} \tag{10}$$

and the total characteristic velocity for the idealized transfer in the normalized form is

$$\Delta v_i = \Delta v_{di} + \Delta v_{ci} \tag{11}$$

(iii) Realistic Aeroassisted Transfer

In a realistic, aeroassisted, coplanar transfer, the vehicle is transferred from HEO at R_d to LEO at R_c, by flying deep into the atmosphere to achieve the necessary velocity reduction (Figure 3). We start with a tangential propulsive burn, having a characterstic velocity ΔV_d for deorbitting from the high Earth orbit (HEO) and entering into an elliptical transfer orbit. At point E the spacecraft enters the sensible atmosphere with an inclination of γ_e and undergoes reduction in velocity due to atmospheric drag. At point F, the spacecraft leaves the atmosphere with flight path angle γ_f. Once again, the transfer orbit is elliptical with the corresponding apogee at R_c. Finally, the maneuver ends with a cirularize or reorbit burn having a characteristic velocity ΔV_c to make the vehicle enter into the low Earth orbit. The desired circularization into LEO is achieved by the appropriate magnitude of ΔV_c. Thus, the maneuver consists of two impulses ΔV_d for deorbit, and ΔV_c for circularization. Upon applying the principles of conservation of angular momentum and the conservation of energy, we obtain the relations for the deorbit and the circularization impulses as

$$\Delta V_d = \sqrt{\mu/R_d}\left[1 - \sqrt{2(1-R_d/R_a)/\left(1-(R_d/R_a)^2/\cos^2\gamma_e\right)}\right] \tag{12}$$

$$\Delta V_c = \sqrt{\mu/R_c}\left[1 - \sqrt{2(1-R_c/R_a)/\left(1-(R_c/R_a)^2/\cos^2\gamma_f\right)}\right] \tag{13}$$

In terms of the normalized values (3),

$$\Delta v_d = \sqrt{1/a_d} - \sqrt{2(1-a_d)/a_d(1-a_d^2/\cos^2\gamma_e)} \tag{14}$$

$$\Delta v_c = \sqrt{1/a_c} - \sqrt{2(1-a_c)/a_c(1-a_c^2/\cos^2\gamma_f)} \tag{15}$$

Finally, the total characteristic velocity for the realistic aeroassisted transfer in the normalized form becomes

$$\Delta v = \Delta v_d + \Delta v_c \tag{16}$$

Let us note that if $\gamma_e = \gamma_f = 0$, the relations (12) to (16) for the various characteristic velocities for the realistic transfer are the same as those relations (7) to (11) for the corresponding characteristic velocities for the idealized transfer. Thus, the total characteristic velocity Δv for the

realistic transfer is atleast equal to that of Δv_1. In otherwords, the idealized transfer is the lower bound of the realistic transfer.

The entry velocity v_e, and the exit velocity v_f are also obtained in the normalized form as

$$v_e = \sqrt{2a_d(1-a_d)/(\cos^2\gamma_e - a_d^2)} \tag{17}$$

$$v_f = \sqrt{2a_c(1-a_c)/(\cos^2\gamma_f - a_c^2)} \tag{18}$$

(iv) Comparison of Orbital Transfers

We now try to compare the three types of transfers, i.e., Hohmann transfer, ideal aeroassisted transfer, and realistic aeroassisted transfer. For this, the following date is used. Radius of Earth, R_E = 6,378 KM ;radius of atmosphere, R_a = 6,498 KM; radius of the HEO, R_d = 42,241 KM; radius of the LEO, R_c = 6,728 KM; gravitational constant of Earth, $\mu = 3.986 \times 10^{14}$ meter^3/sec^2. Using this data, the deorbit and circularization velocities and the total characteristic velocities for each of the types of transfers is shown in Figure 4. The variation of entry velocity V_e and the deorbit characteristic velocity ΔV_d with respect to entry flight path angle γ_e are depicted in Figure 5. Also, the variation of exit velocity V_f and the reorbit characteristic velocity ΔV_f are shown in Figure 6. The effect of altitude of LEO H_c, on the reorbit characteristic velocity ΔV_c is shown in Figure 7. As expected, the minimum ΔV_c at γ_c increases with the altitude of LEO. The scenario at the entry and exit corridors shown in Figures 5 and 6 indicate that we need to fly the vehicle at near zero exit flight path angle for minimum fuel consumption.

3. EQUATIONS OF MOTION

Consider a vehicle with constant point mass, moving about a nonrotating spherical planet. The atmosphere surrounding the planet is assumed to be at rest, and the central gravitational field obeys the usual inverse square law. The equations of motion are given by,

$$\frac{dH}{dt} = V\sin\gamma \tag{19a}$$

$$\frac{dV}{dt} = -AC_D V^2 \exp(-H\beta) - (\mu/R^2)\sin\gamma \tag{19b}$$

$$\frac{d\gamma}{dt} = AC_L V\exp(-H\beta) + [V/R - \mu/(R^2V)]\cos\gamma \qquad (19c)$$

where $A = S\rho_s/2m$, $H = R-R_s$, $\rho = \rho_s\exp(-H\beta)$ and

$C_D = C_{DO} + KC_L^2$ for a drag polar.

Using the normalized variables,

$$\tau = t/\sqrt{R_a^3/\mu} \; ; \quad v = V/\sqrt{\mu/R_a} \qquad (20)$$

and the dimensionless constants,

$$h = H/H_a; \quad b = R_a/H_a; \quad \delta = \rho/\rho_s = \exp(-h\beta H_a); \qquad (21a)$$

$$c = C_L/C_{LR}; \quad C_{LR} = \sqrt{C_{DO}/K} \qquad (21b)$$

$$\frac{dh}{d\tau} = bv\sin\gamma \qquad (22a)$$

$$\frac{dv}{d\tau} = - A_1 b(1+c^2)\delta v^2 - \frac{b^2\sin\gamma}{(b-1+h)^2} \qquad (22b)$$

$$\frac{d\gamma}{d\tau} = A_2 bc\delta v + \frac{bv\cos\gamma}{(b-1+h)} - \frac{b^2\cos\gamma}{(b-1+h)^2 v} \qquad (22c)$$

where, $A_1 = C_{DO}S\rho_s H_a/2m$; $A_2 = C_{LR}S\rho_s H_a/2m$

4. OPTIMAL CONTROL

For an optimal control problem with minimum fuel consumption, it is required to choose the performance index to minimize the total characteristic velocity, which is the sum of the initial characteristic velocity ΔV_d, the deorbit impulse from HEO, and the final characteristic velocity ΔV_c, the circularization impulse into LEO. Thus, the performance index is given by [6]

$$J = \Delta V = \Delta V_d + \Delta V_c \qquad (23)$$

where $\Delta V_d = \sqrt{\mu/R_d} - (R_a/R_d)V_e\cos(-\gamma_e)$

$$\Delta V_c = \sqrt{\mu/R_c} - (R_a/R_c)V_f\cos\gamma_f$$

In the normalized form, the performance index becomes,

$$J = \Delta v = \Delta v_d + \Delta v_c \tag{24}$$

where,

$$\Delta v_d = \sqrt{1/a_d} - (v_e/a_d)\cos(-\gamma_e)$$

$$\Delta v_c = \sqrt{1/a_c} - (v_f/a_c)\cos(\gamma_f)$$

Alternatively, the expressions for ΔV_d and ΔV_c are given by (12) and (13). The minimization of J with respect to γ_e and γ_f yields $\gamma_e = 0$ and $\gamma_f = 0$. Because of this, it is natural to postulate that the optimal trajectory behaves as $\gamma(t) = 0$ for all values of time t between the entry time t_e and the exit time t_f. This constant flight path angle along the trajectory means that the altitude is constant at the value equal to altitude of the atmospheric interface. Thus, the optimal trajectory becomes an ideal (grazing) trajectory.

We are interested in finding the minimization of the fuel with respect to the control C_L. Using Pontryagin principle, we formulate Hamiltonian as

$$\mathcal{H} = \lambda_h bv\sin\gamma + \lambda_v\left\{A_1 b(1+c^2)\delta v^2 - \frac{b^2\sin\gamma}{(b-1+h)^2}\right\}$$

$$+ \lambda_\gamma\left\{A_2 bc\delta v + \frac{bv\cos\gamma}{(b-1+h)} - \frac{b^2\cos\gamma}{(b-1+h)^2 v}\right\} \tag{25}$$

where λ_h, λ_v, and λ_γ are the costates (Lagrange multipliers) corresponding to the states h, v, and γ respectively.

The unconstrained optimal control is obtained from

$$\frac{\partial \mathcal{H}}{\partial c} = 0 \tag{26a}$$

This leads us to

$$c = E_m \lambda_\gamma / v\lambda_v; \text{ where, } E_m = (L/D)_{max} \tag{26b}$$

Realistically, the control C_L is bounded by the aerodynamic characteristics of the vehicle. Thus, for the contstrained control,

$$|C_L| \leq C_{Lmax} \text{ or } |c| \leq c_{max} \tag{27}$$

The costate (adjoint) variables λ's are solved from

$$\frac{d\lambda_h}{d\tau} = -\frac{\partial \mathcal{H}}{\partial h}; \qquad \frac{d\lambda_v}{d\tau} = -\frac{\partial \mathcal{H}}{\partial v}; \qquad \frac{d\lambda_\gamma}{d\tau} = -\frac{\partial \mathcal{H}}{\partial \gamma} \tag{28}$$

Boundary Conditions

The initial and final boundary conditions are given for the normalized altitude h as

$$h(\tau=0) = 1.0, \quad h(\tau=\tau_f) = 1.0 \tag{29a}$$

and for the normalized velocity v, and the flight path angle γ as

$$(2-v_e^2)a_d^2 - 2a_d - v_e^2\cos^2\gamma_e = 0 \tag{29b}$$

$$(2-v_f^2)a_c^2 - 2a_c - v_f^2\cos^2\gamma_f = 0 \tag{29c}$$

The above relations result from the considerations of energy conservation and angular momentum conservation applied to the HEO-to-entry elliptic transfer orbit and exit-to-LEO elliptic transfer orbit, respectively. The remaining boundary conditions are obtained from the transversality conditons on the costates. Thus, the optimization procedure, requiring the solution of state equations (22) and the corresponding costate equations (28) along with the boudary conditons (29), leads us to the formation of a nonlinear, two-point, boundary value problem (TPBVP), which is solved by using a multiple shooting method.

5. NUMERICAL DATA AND RESULTS

A typical set of numerical values used for simulation purposes is given below [4].

$C_{DO} = 0.21$; $K = 1.67$; $m/S = 300$ kg/m^2
$\rho_s = 1.225$ kg/m^3; $\mu = 3.986\text{x}10^{14}$ m^3/sec^2
$\beta = 1/6900$ m^{-1}; $R_E = 6378$ KM
$H_a = 120$ KM; $R_d = 12996$ KM; $R_c = 6558$ KM

Using the above mentioned data, simulations are carried out. Time histories of altitude H, velocity V, and flight path angle γ, for total flight time of 540 seconds, are shown in Figure 8. Figure 9 shows the lift and the lift-to-drag ratio as a function of time from atmospheric entry to exit points. Those for the heating rate, dynamic pressure and density are shown in Figure 10. The maximum positve L/D is used initially to recover from the

downward plunge. As the flight path angle becomes positve, the maximum negative L/D is used to level off the flight. Then a negative L/D is used to maintain flight at a small positve flight path angle in order to achieve the shallow exit.

Figure 8(a) shows the time history of altitude. The spacecraft enters and exits the atmosphere at an altitude of 120 KM. The minimum altitude reached is 55.56 KM. The velocity versus time is shown in Figure 8(b). The vehicle enters the atmosphere with a velocity of 9029 m/sec and leaves the atmosphere with a speed of 7795 m/sec, thus giving a velocity reduction of 1234 m/sec. The profile of flight path angle with time is shown in Figure 8(c). The spacecraft enters the atmosphere with an inclination of -5.665 degrees and exits with +0.927 degrees. The conrol history is shown is shown in Figure 9(a). The vehicle enters the atmosphere with maximum lift capability and switches to the minimum lift coefficient and then gradually increases during the ramaining flight.

The minimum-fuel transfer requires a deorbit (impulse) characteristic velocity ΔV_d of 1034.29 m/sec and a reorbit characteristic velocity ΔV_c of 73.25 m/sec, with a total characteristic velocity of 1107.54 m/sec. Let us compare this aeroassisted transfer with the Hohmann transfer, which is maneuvered entirely in outer space, and has a deorbit characteristic velocity ΔV_{dh} of 1002.39 m/sec and the reorbit characteristic velocity ΔV_{ch} of 1192.25 m/sec, giving a total characteristic velocity for Hohmann transfer ΔV_h of 2194.64 m/sec. This shows that the saving due to coplanar, aeroassisted transfer over Hohmann transfer is 49.54 pecent. In the case of idealized transfer which follows a grazing trajectory along the atmospheric boundary, the deorbit characteristic velocity ΔV_{di} is 1016.24 m/sec and reorbit characteristic velocity ΔV_{ci} is 17.94 m/sec, thus giving a total characteristic velocity of 1034.18 m/sec. The optimal transfer requires only 6.63 percent more fuel than that of the idealized transfer.

The heating rate Q_r, along the atmospheric trajectory, is computed for a sphere of radius of 1 meter, according to the relation [3],

$$Q_r = K_r \rho^{0.5} V^{3.08} \qquad (30)$$

where, ρ is the atmospheric density in kg/km^3, V is the velocity in km/sec and K_r is the proportionality constant equal to 3.08×10^{-4}. Figure 10(a) shows peak heating rate of 129.2 W/sq.cm. and the total integrated heating rate is found to be 15.536 KW-sec/cm^2. As shown in Figure 10(b), the peak dynamic pressure is 26.73 kN/sq.m. The variation of density in Figure 10(c) attains a maximum value of 0.3902 kg/m^3.

Entry Corridor

A concept associated with atmospheric entry trajectories is that of the entry corridor. This is required due to the fact that a given vehicle cannot fly an acceptable atmospheric flight for orbitrary initial conditons at the

entry point. If the flight path angle γ_e is too steep, the vehicle will later suffer excessive aerodynamic and aerothermodynamic loadings even if the maximum lift is directed upward. This also may lead to "crash" condition. Or if the entry flight path angle is too shallow, the vehicle will exit the atmosphere again with an orbital velocity even if the maximum lift is directed downward. This leads to "escape" or uncontrolled skip-out condition. These boudaries of entry flight path angle are often taken to define the corridor of acceptable entry conditions. The responsibility of generating acceptable entry corridor lies largley with the last phase of the midcourse guidance system. Without a proper midcourse correction, it will be beyond the capability of the atmospheric flight control system to fly a safe trajectory.

The entry corridor is the entry interface undershoot and overshoot and is usually specified by the entry flight path angle γ_e, as dictated by the entry dynamics. In the present case of fuel-optimal, coplanar, orbital transfer, four simulations are carried out as shown in Table I below. Figure 11 shows the entry corridor with flight path angle ranging from -7.24 deg -5.485 degrees.

Table I:

Simulation No	γ_e deg	V_e m/sec	C_L	flight time seconds
1	-7.240	9020	0.5381	510
2	-6.412	9025	0.5786	600
3	-5.665	9029	0.6299	540
4	-5.485	9030	0.6502	600

Approximate Solutions

As a first cut in getting approximate solutions, we try to obtain the optimal solutions using the fact that the flight path angle γ is small. Using this approximation, the simulation has been repeated. Interestingly, it is found that we get almost the identical solutions with much less computation time. For example, in this case, the deorbit characteristic velocity ΔV_d is equal to 1034.29 m/sec, and the reorbit characteristic velocity ΔV_c is found to be 73.26 m/sec, giving a total minimum characteristic velocity as 1107.55 m/sec. The total integrated heating rate is 15.556 KW-sec/cm^2. The execution time on the computer is now only 59.2 percent of the execution time for the optimal solution without the approximation.

6. MULTIPLE SHOOTING METHOD

The determination of optimal control (26) requires the solution of a sixth order, nonlinear TPBVP consisting of state equations (22) and costate equations (28) and the associated boundary conditions (29). This can only be done by numerical methods. The multiple shooting method is one of the

powerful methods for solving nonlinear TPBVP's. The corresponding OPTSOL code was developed by DFVLR establishment at Oberpfaffenhofen, West Germany [7,8].

In solving any boundary value problem with the given initial and final conditions, we asume additional initial data and integrate forward so that the solution satisfies the given final condition as well. This is also called a simple shooting method. Here, the convergence of the solution is highly sensitive to the assumed intial data. It is found that the error due to inaccurate initial data can be made arbitrarily small by performing the integration over sufficiently smaller subdivided panels within the given interval and thereby leading to the multiple shooting method. Thus, the multiple shooting method is a simultaneous application of the simple shooting method at several points within the interval of integration. Here, the trajectory may be restarted at intermediate points using new guesses. Jacobian matrices are formed for each segment. The resulting iteration scheme, based on reducing all discontinuties at internal grid points to zero, leads to a system of linear algebraic equations.

Figure 12 shows the successive approximations of the altitude H, during the course of 0, 5, and 14 iterations. For the sake of clarity only 4 out of 20 intervals are shown. The initial guessed value for the altitude is 120 KM at every interval. It can be seen how the intitially large jumps at the subdivision points of the multiple shooting method are "flattened out" with the increase of iterations.

7. CONCLUSIONS

A breif treatment of the three types of orbital transfers, Hohmann transfer, idealized transfer, and realistic transfer, established the fact that the realistic transfer is the upper bound of the idealized (grazing) transfer.

In this report, we have addressed the mimimization of fuel consumption during the atmospheric portion of an aeroassisted, coplanar, orbital transfer vehicle. The resulting two-point, boundary value problem was solved by using an efficient multiple shooting algorithm. Simulations have been carried out to establish a corridor of entry conditions suitable for flying the vehicle through the atmosphere. The strategy for the atmospheric portion of the minimum-fuel transfer is to fly at the maximum L/D initially in order to recover from the downward plunge, and then to fly at a negative L/D to level off the flight such that the vehicle skips out of the atmosphere with a flight path angle near zero degrees.

ACKNOWLEDGEMENTS

This research work was supported by a grant from NASA Langley Research Center, Hampton, under the technical monitorship of Dr Douglas B. Price, Assistant Head, Spacecraft Control Branch.

8. REFERENCES

1. Poineering the Space Frontier, The Report of the National Space Commission on Space, Banton Books Inc., New York, May 1986.

2. Walberg, G. D., "A survey of aeroassisted orbital transfer", J. Spacecraft, 22, pp.3-18, Jan.-Feb., 1985.

3. Mease, K. D., and Vinh, N. X., "Minimum-fuel aeroassisted coplanar orbit transfer using lift modulation", J. Guidance, Control, and Dynamics, Vol., 8, pp.134-141, Jan.-Feb., 1985.

4 Miele, A., Basapur, V. K., and Lee, W. Y., "Optimal trajectories for aeroassisted coplanar orbit transfer", J. Opt. Theory & Appl., 52, pp.1-24, Jan., 1987.

5. Kaplan, M. H., Modern Spacecraft Dynamics and Control, John Wiley & Sons, New York, 1976.

6. Marec, J. P., Optimal Space Trajectories, Elsevier Scientific Publishing Comapany, Amsterdam, 1979.

7. Stoer, J., and Bulirsch, R., Introduction to Numerical Analysis,, Springer-Verlag, New York, 1980.

8. Pesch, H. J., "Numerical computation of neighboring optimum feedback control schemes in real-time", Appl. Math. Optim., 5, pp.231-252, 1979.

****

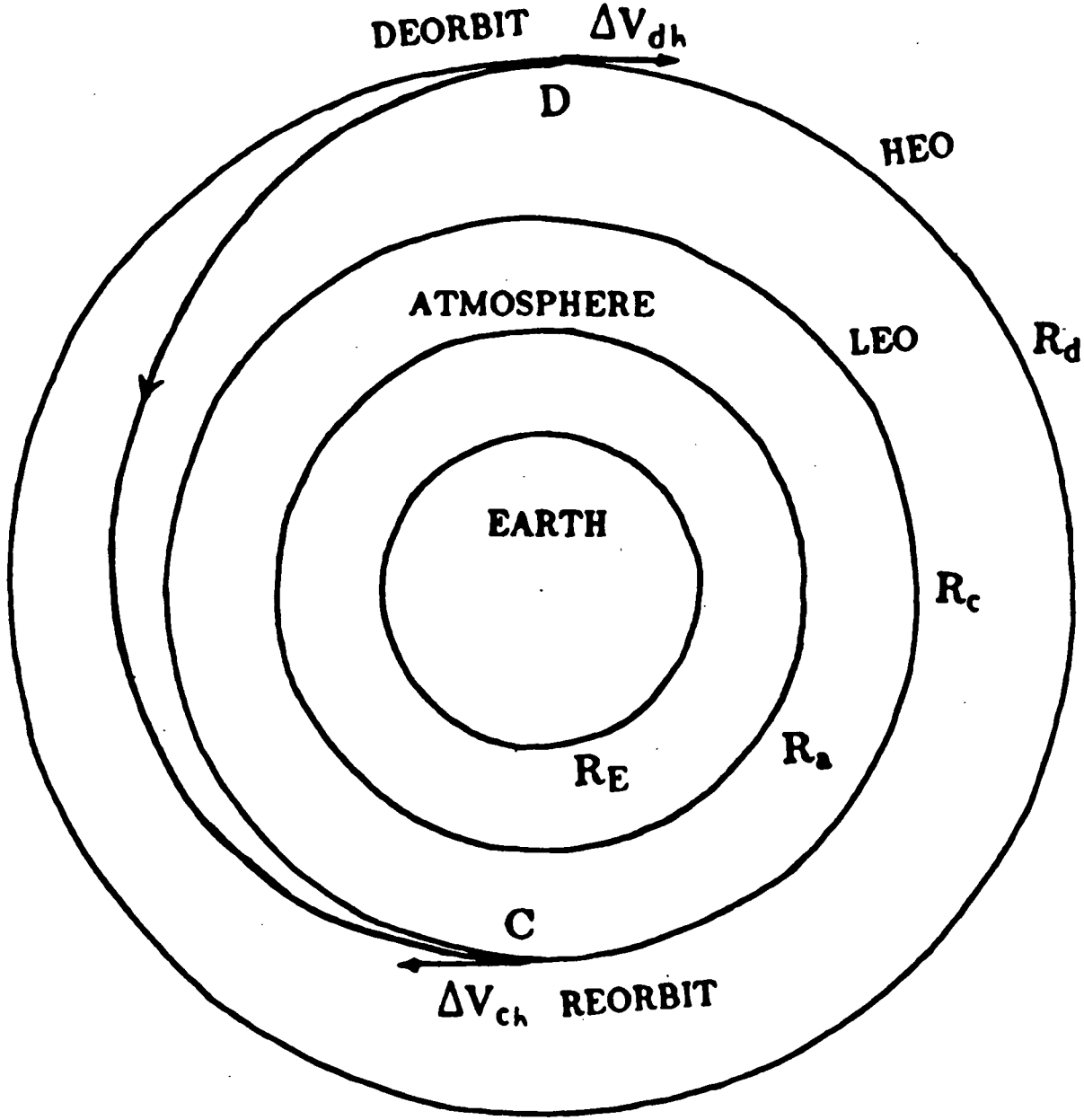

Fig.1 Hohmann transfer

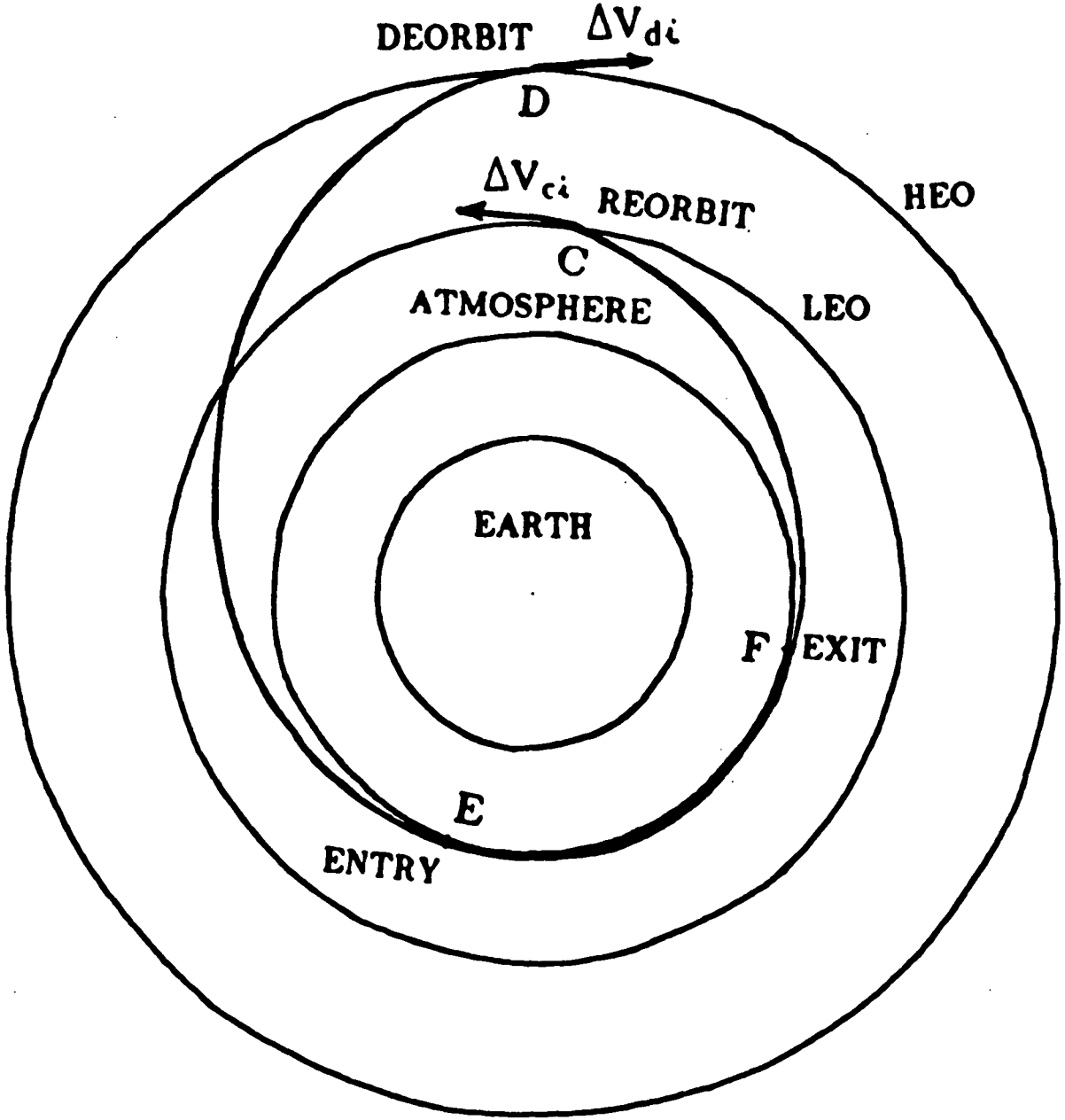

Fig.2 Ideal aeroassisted transfer

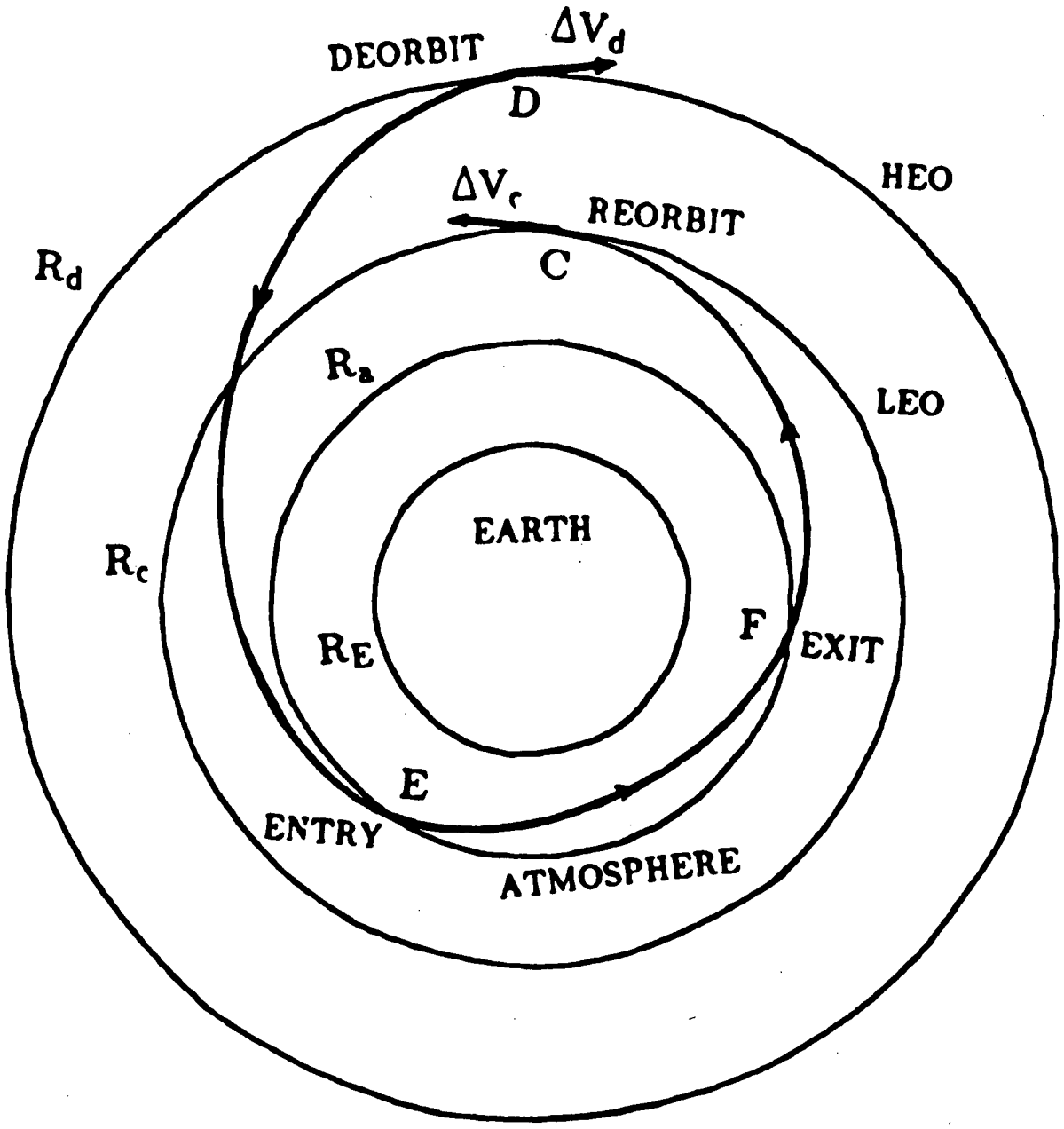

Fig.3 Aeroassisted coplanar orbital transfer

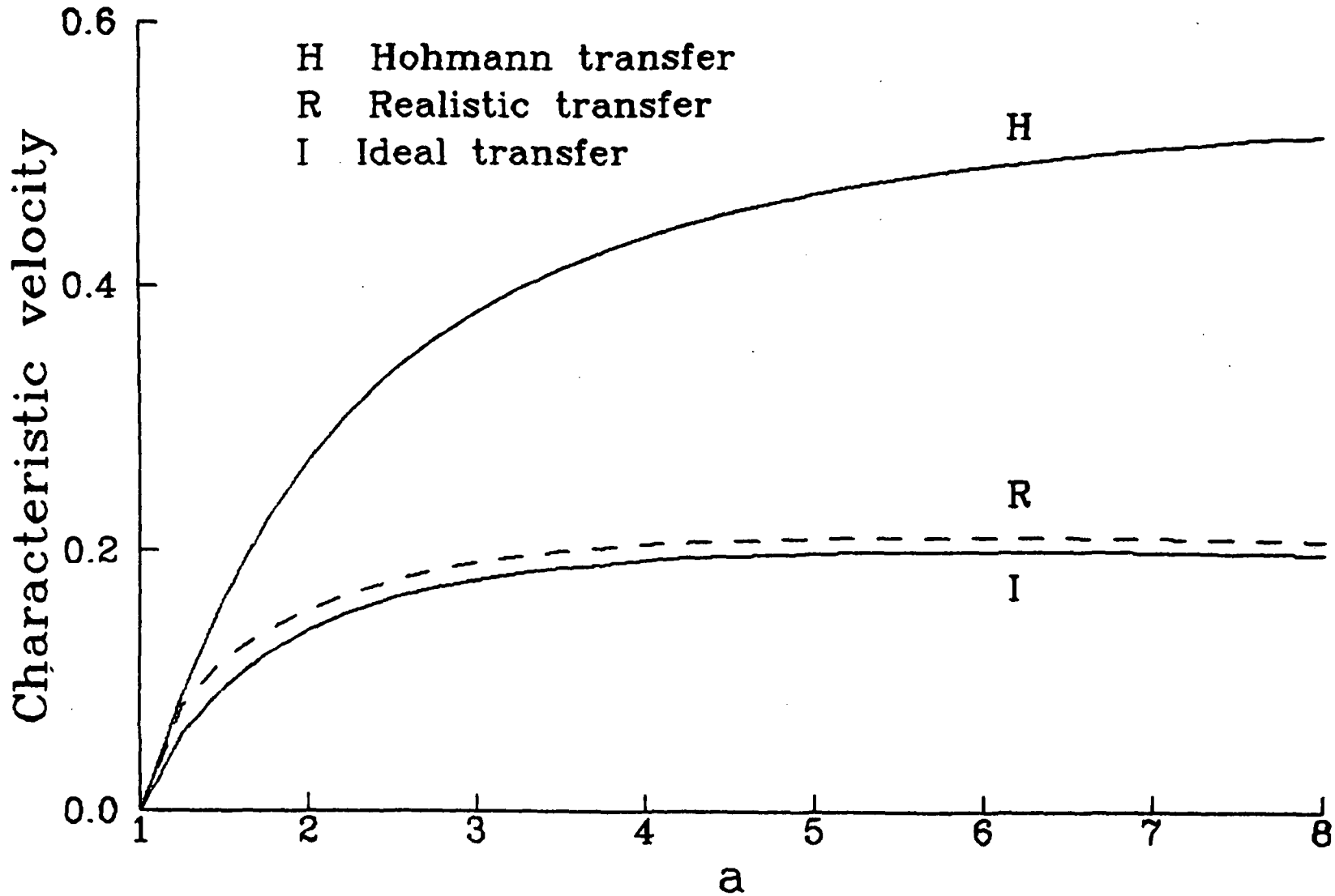

Fig.4 Comparison of orbital transfers

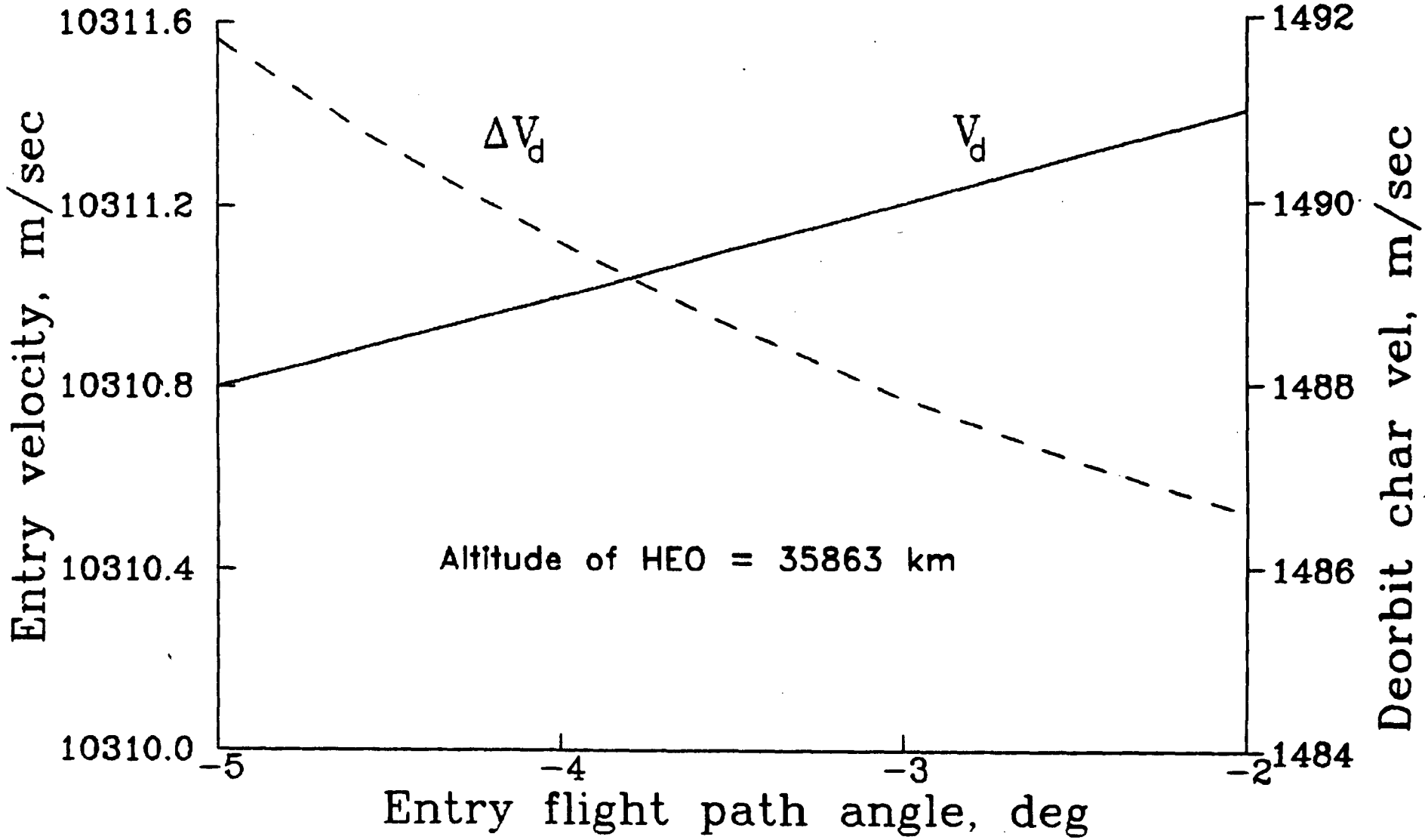

Fig.5 Relations at the entry corridor

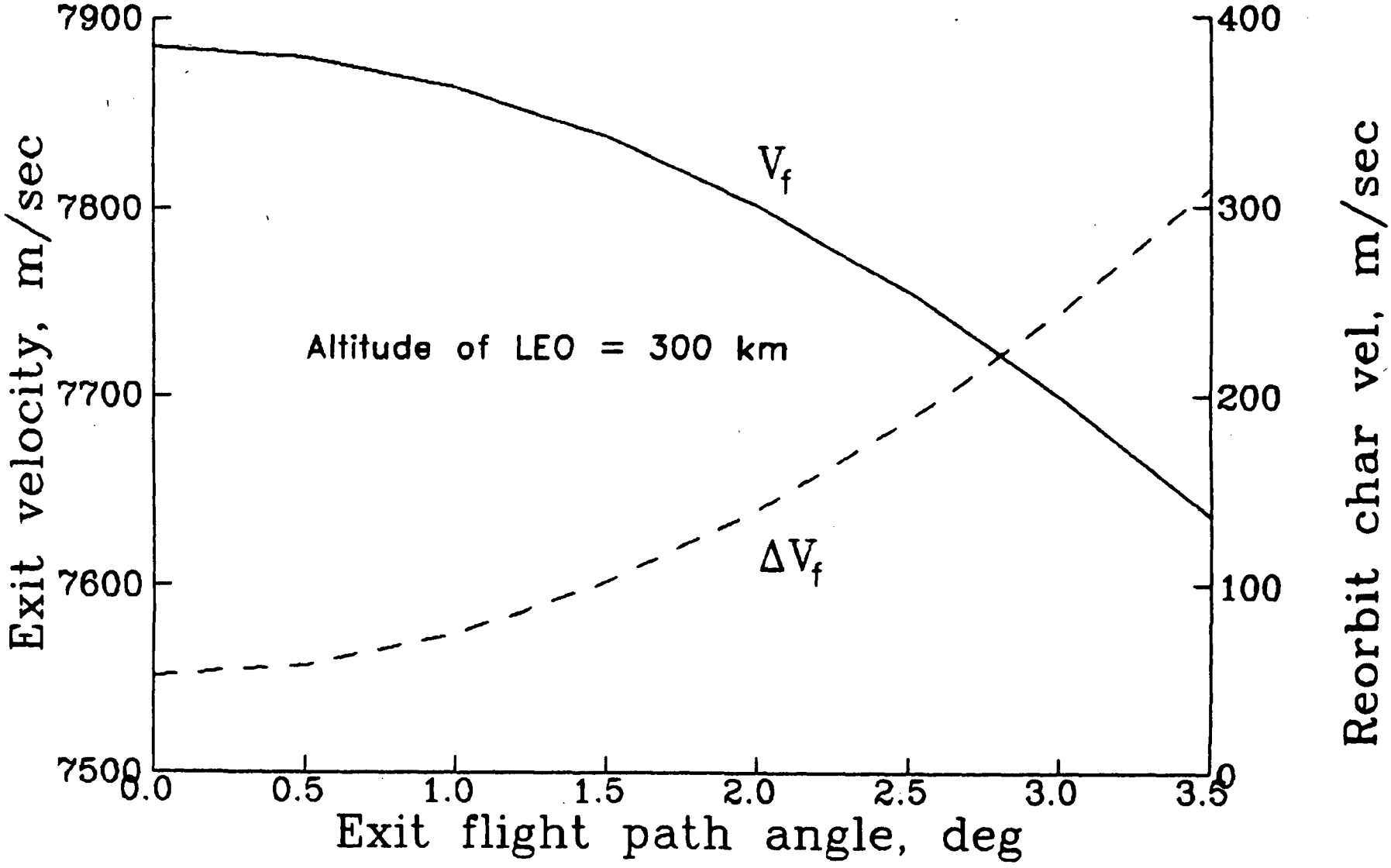

Fig.6 Relations at the exit corridor

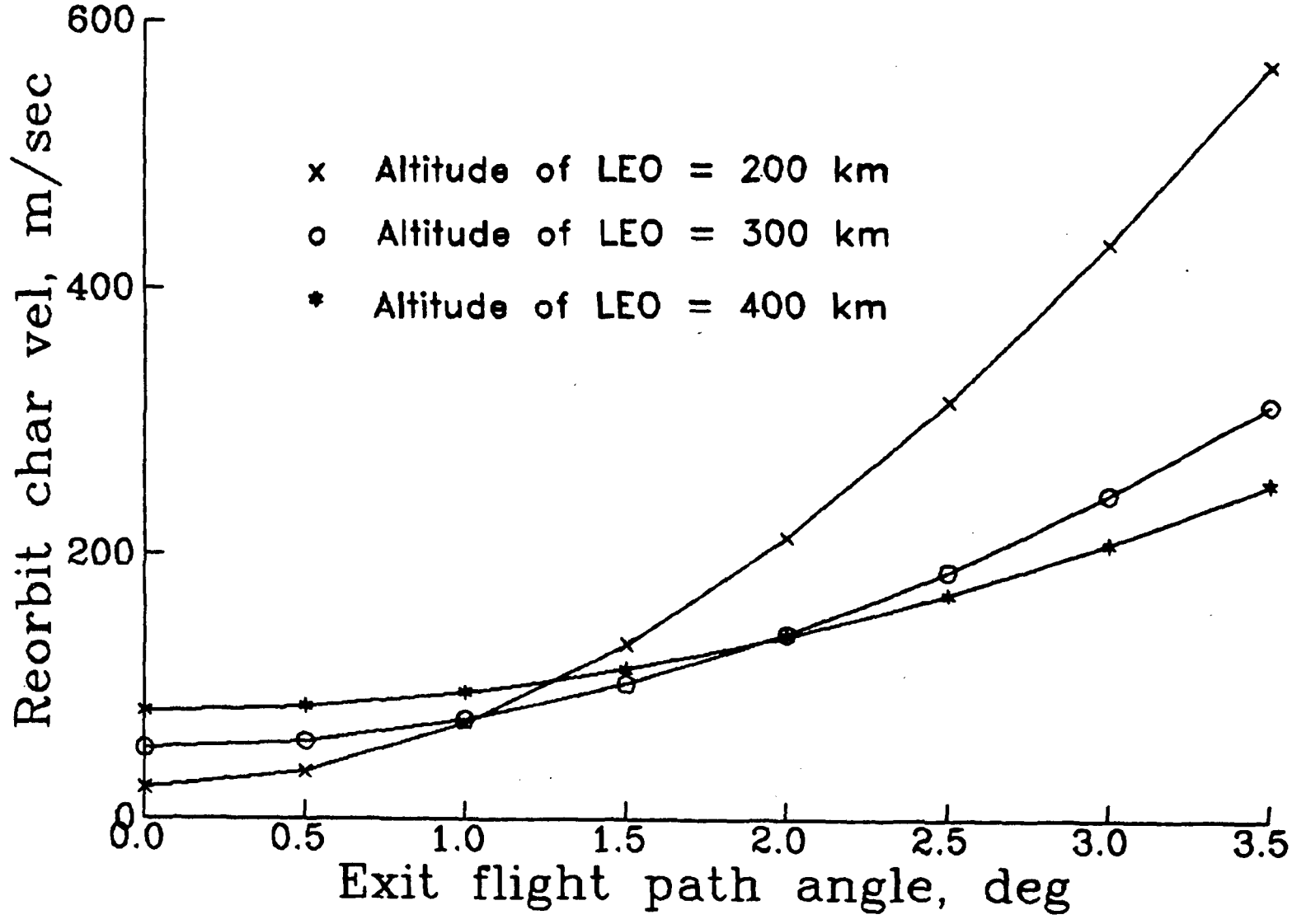

Fig.7 Effect of LEO on reorbit characteristic velocity

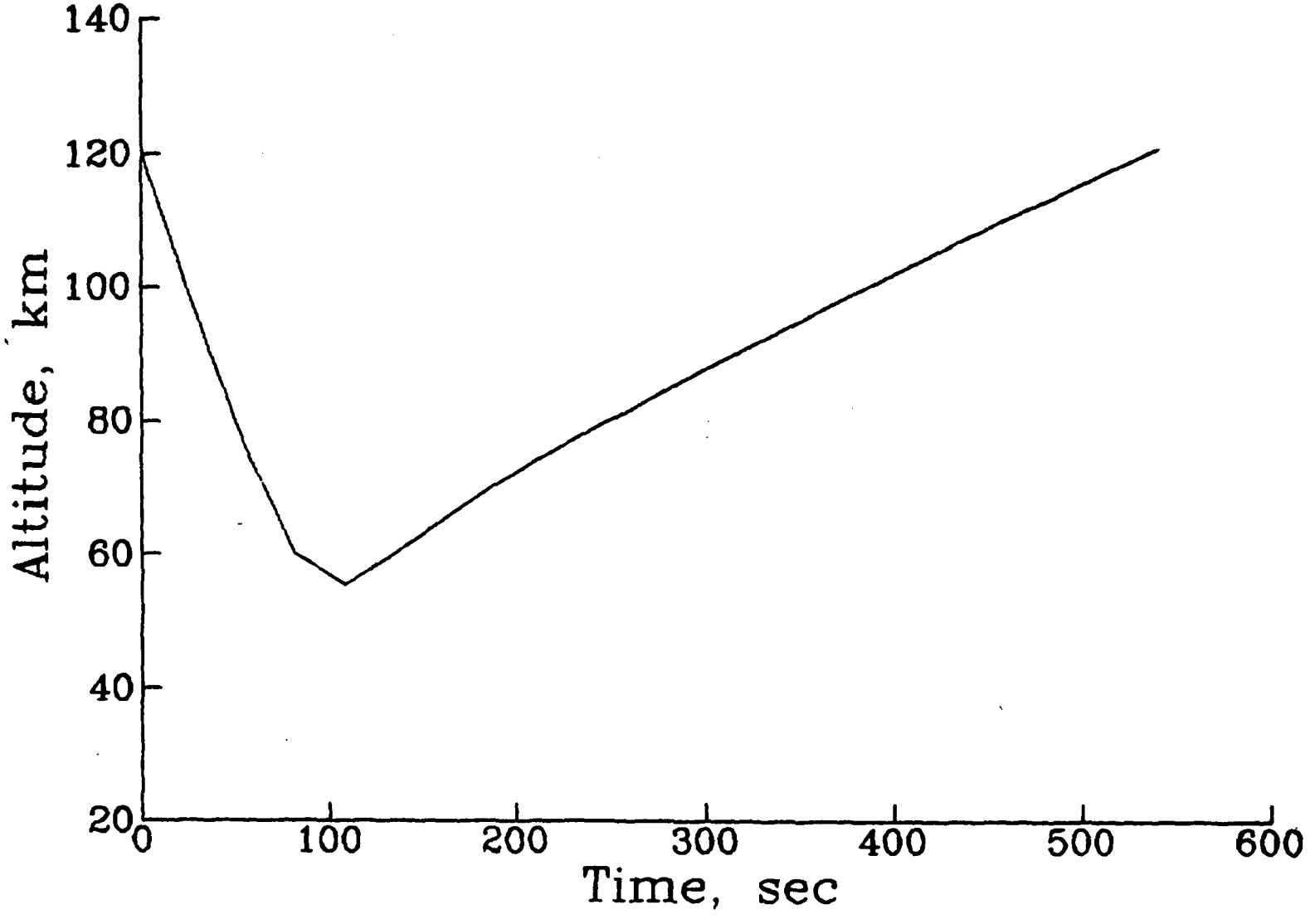

Fig.8(a) Time history of altitude

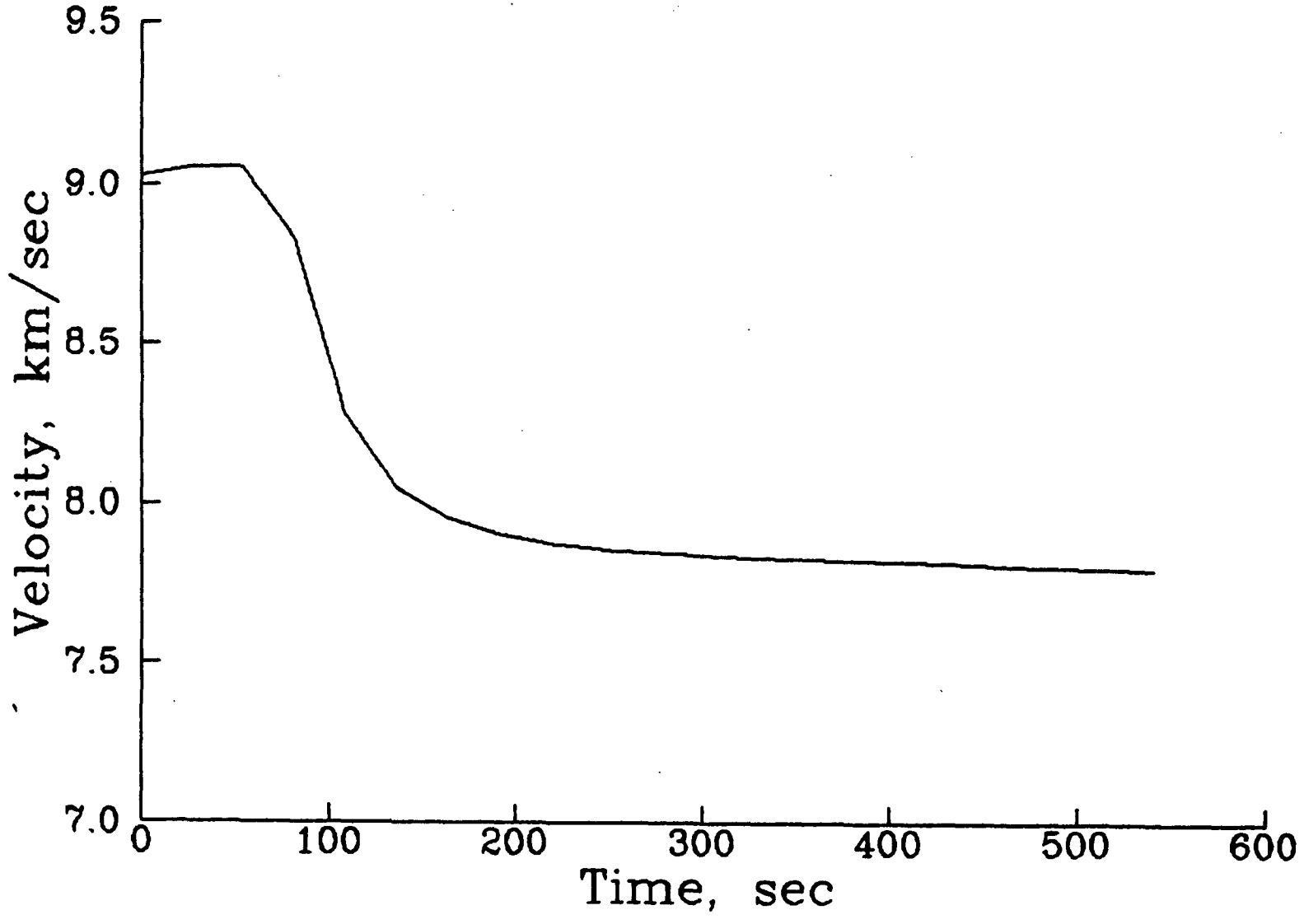

Fig.8(b) Time history of velocity

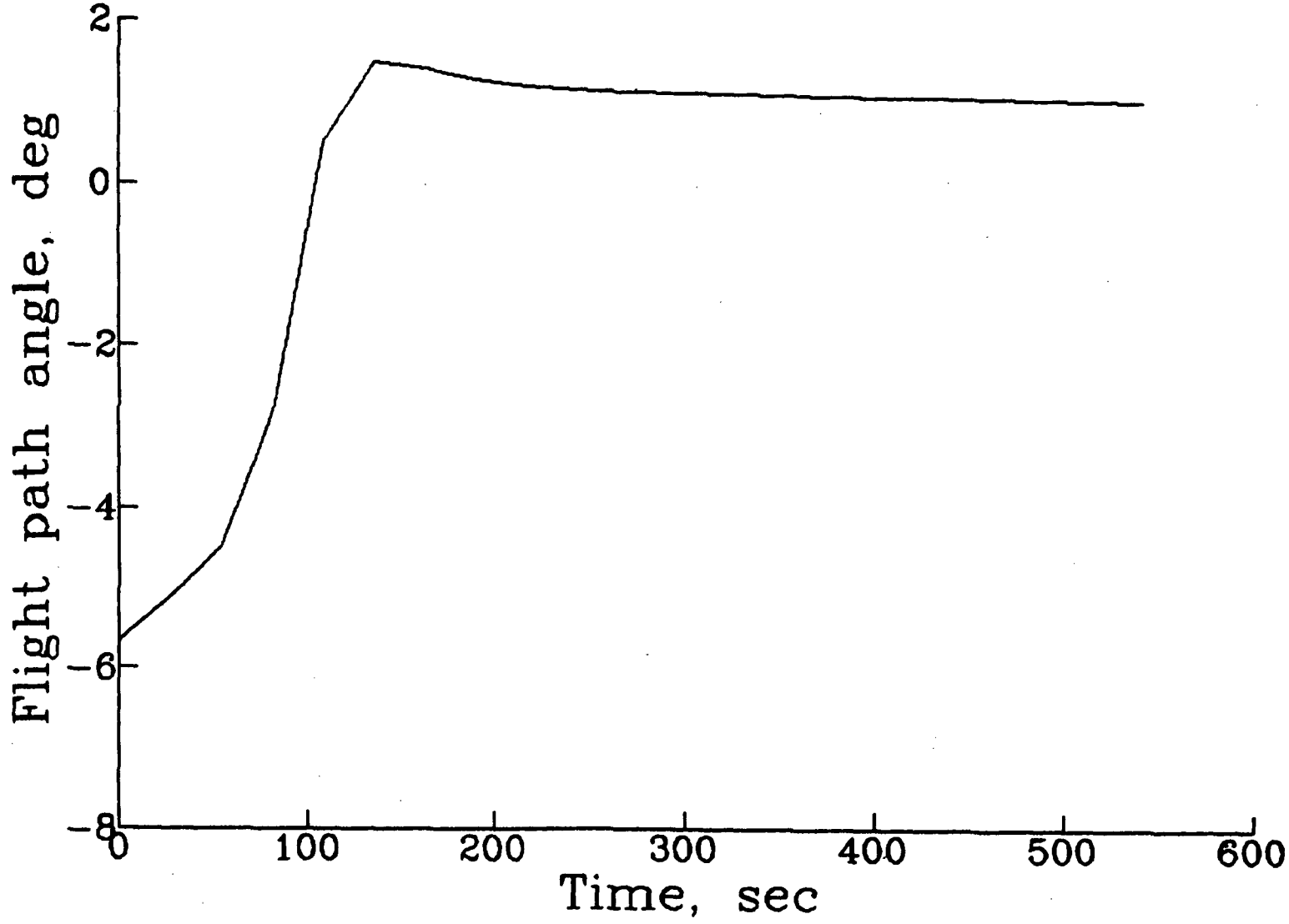

Fig.8(c) Time history of flight path angle

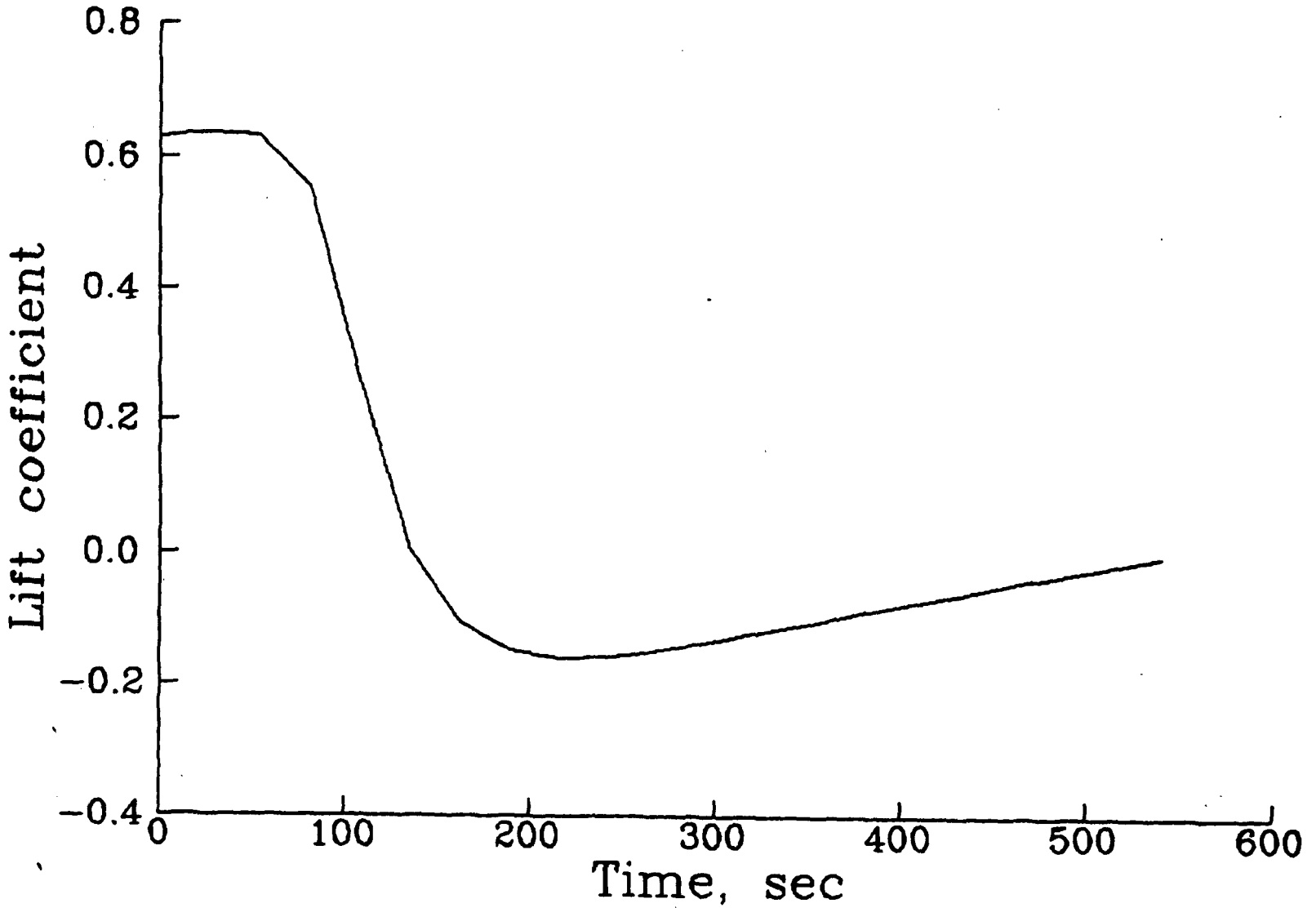

Fig.9(a) Time history of lift coefficient

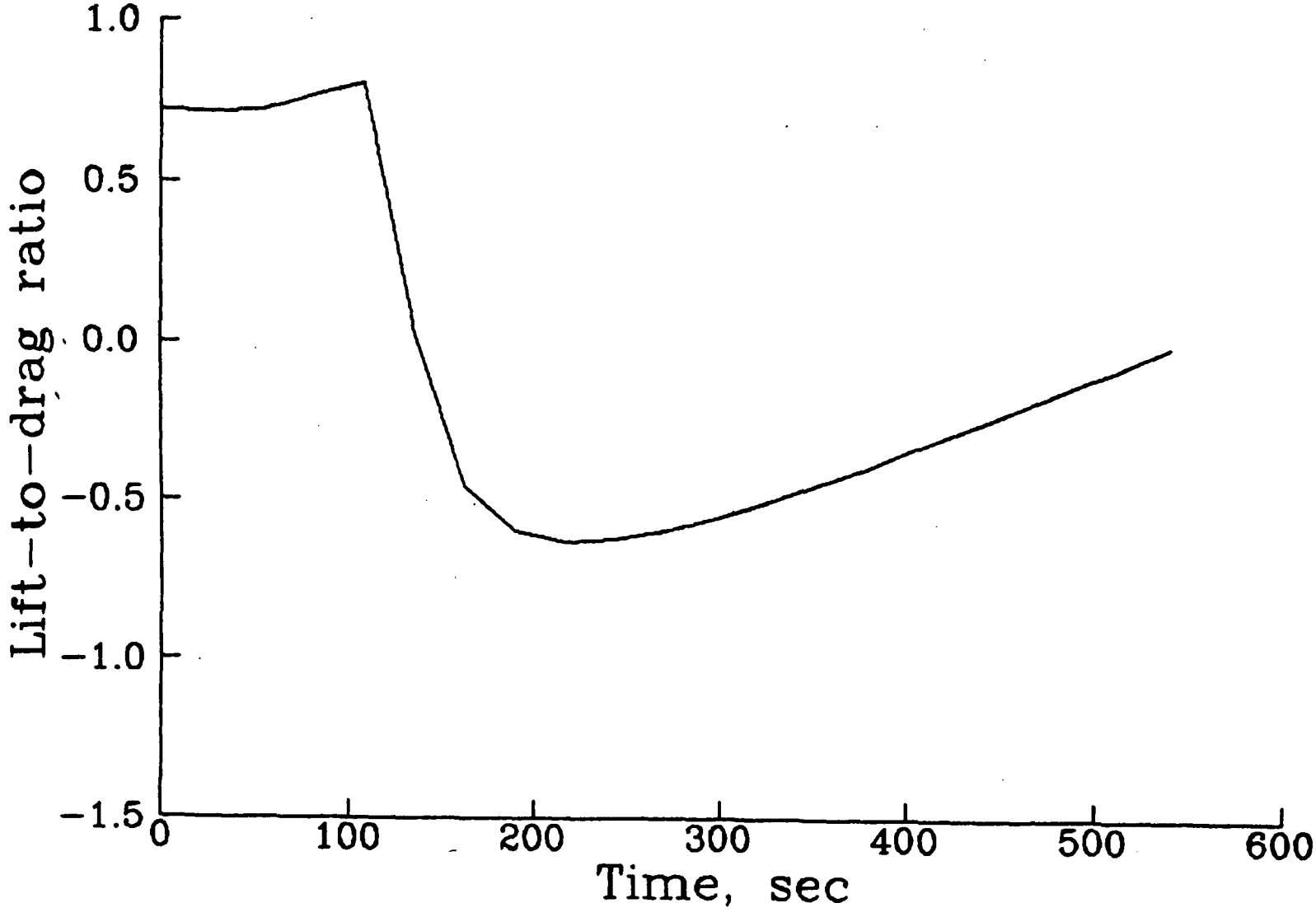

Fig.9(b) Time history of lift−to−drag ratio

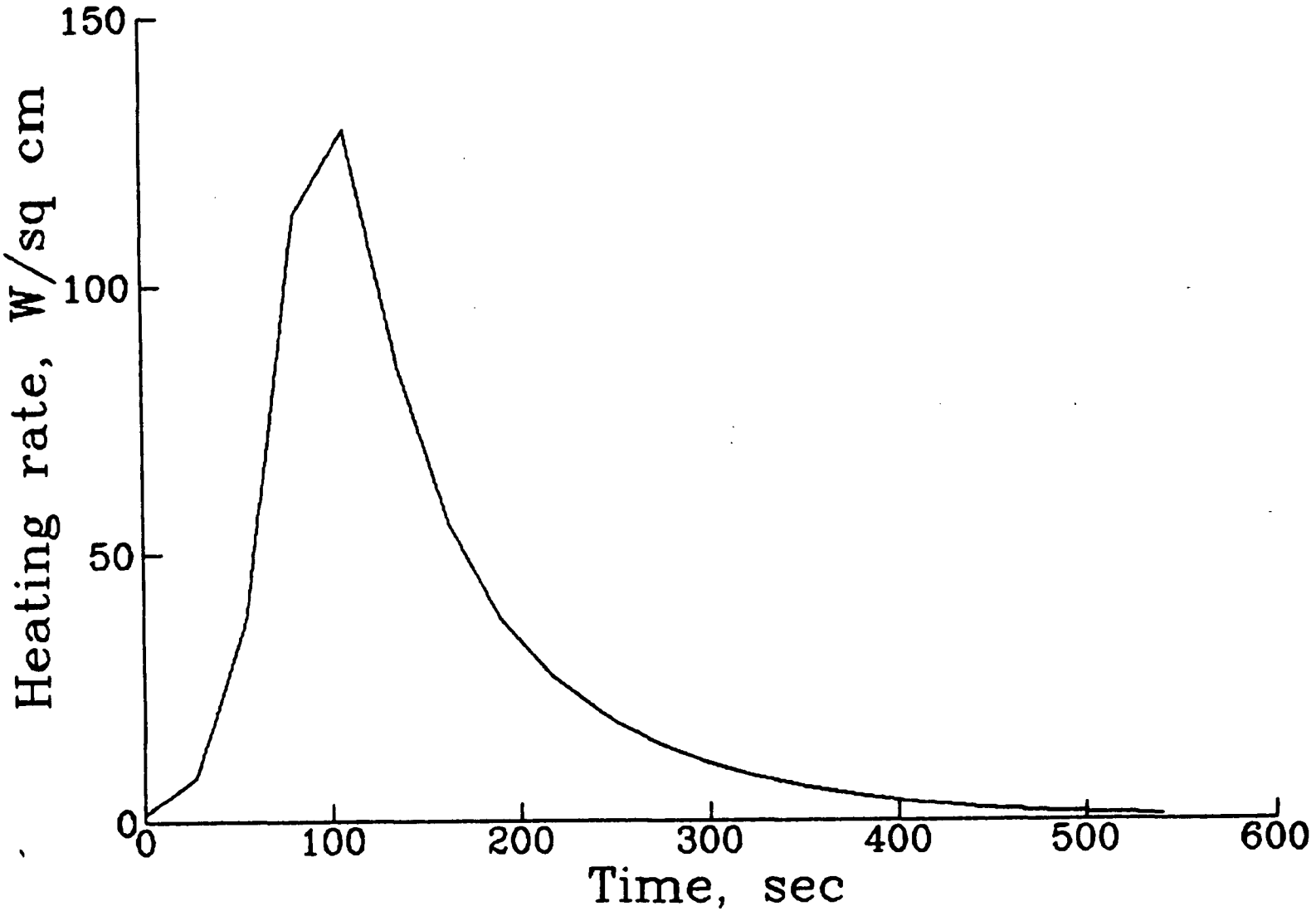

Fig.10(a) Time history of heating rate

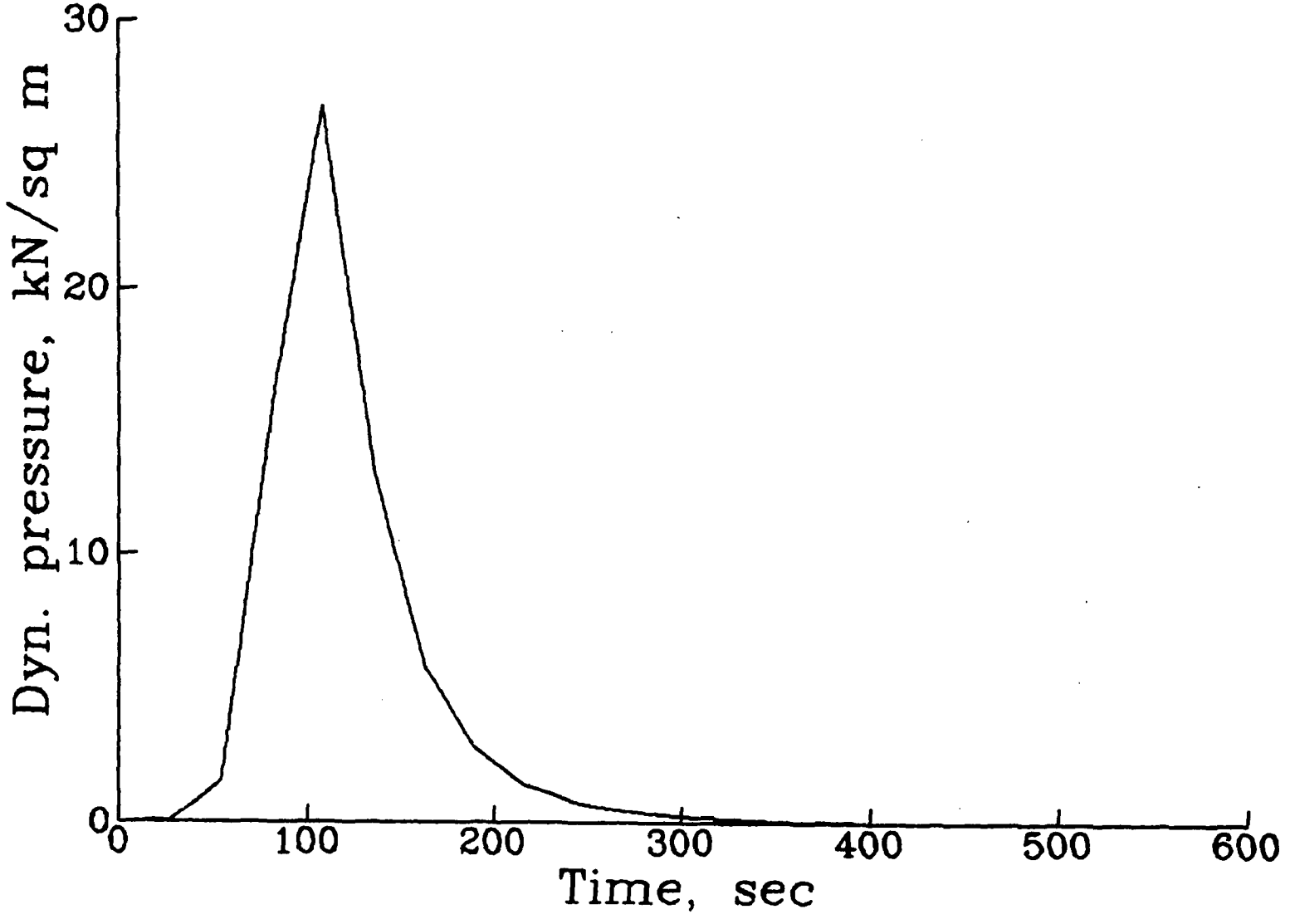

Fig.10(b) Time history of dynamic pressure

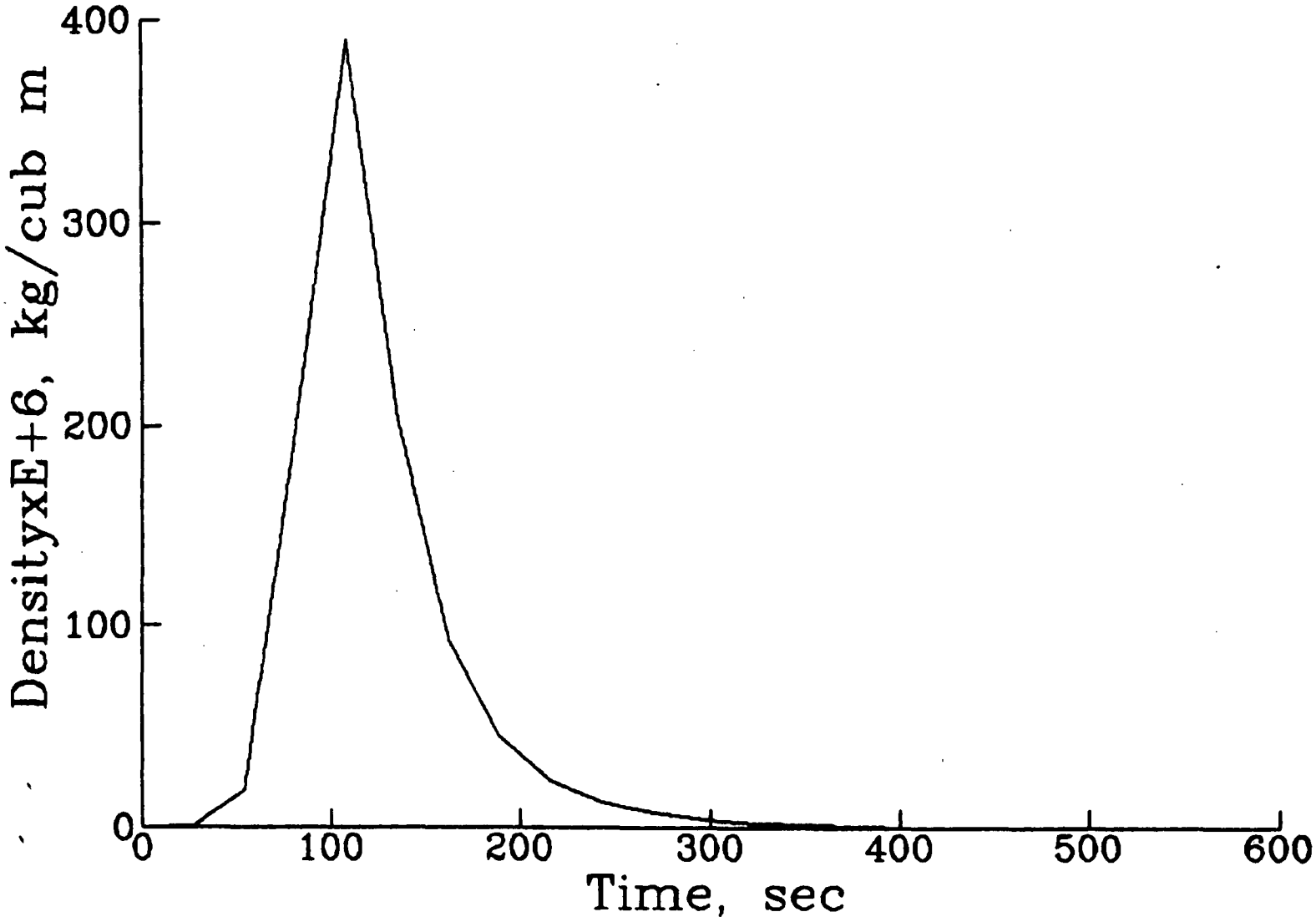

Fig.10(c) Time history of density

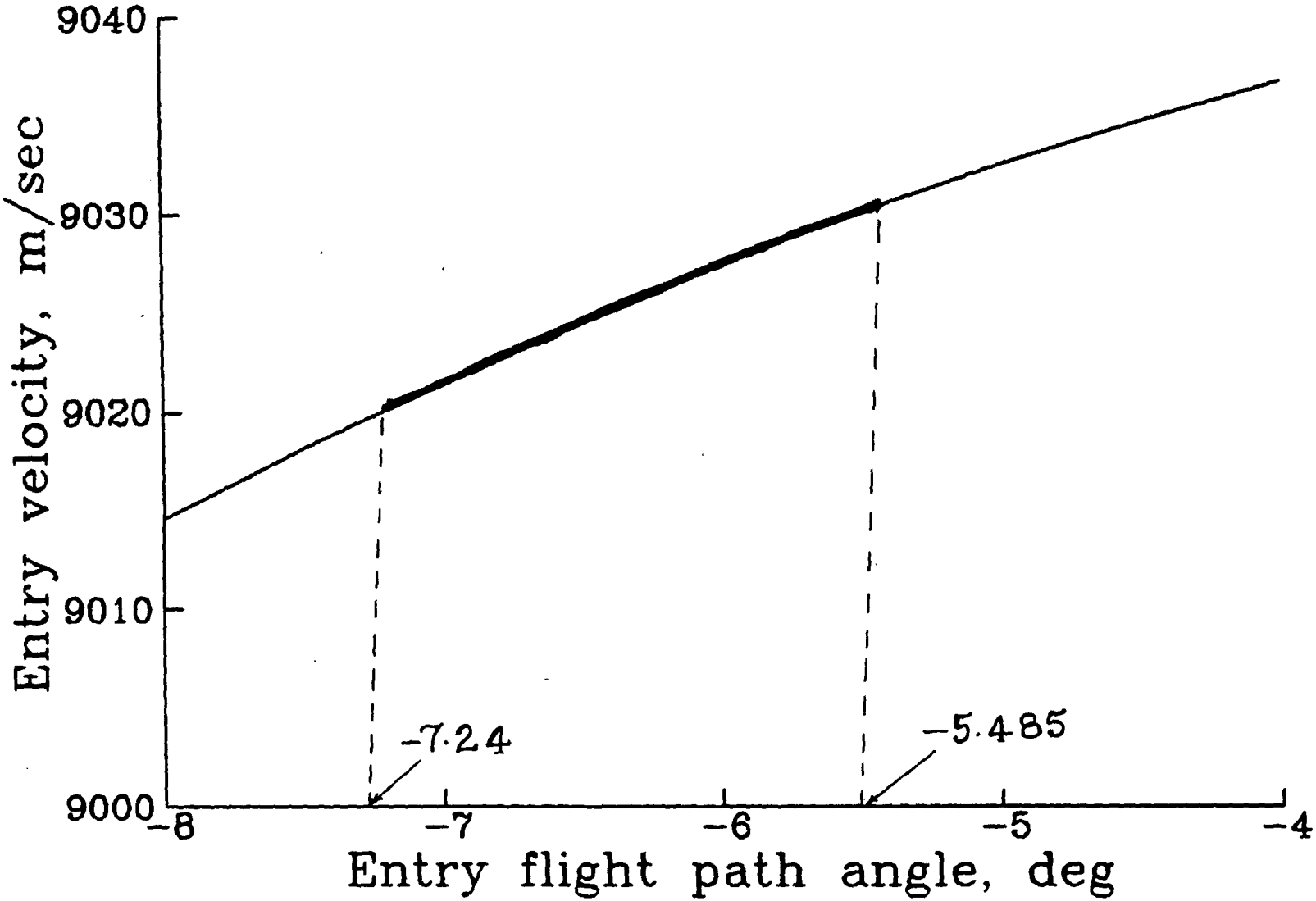

Fig.11 Entry corridor for optimal fuel

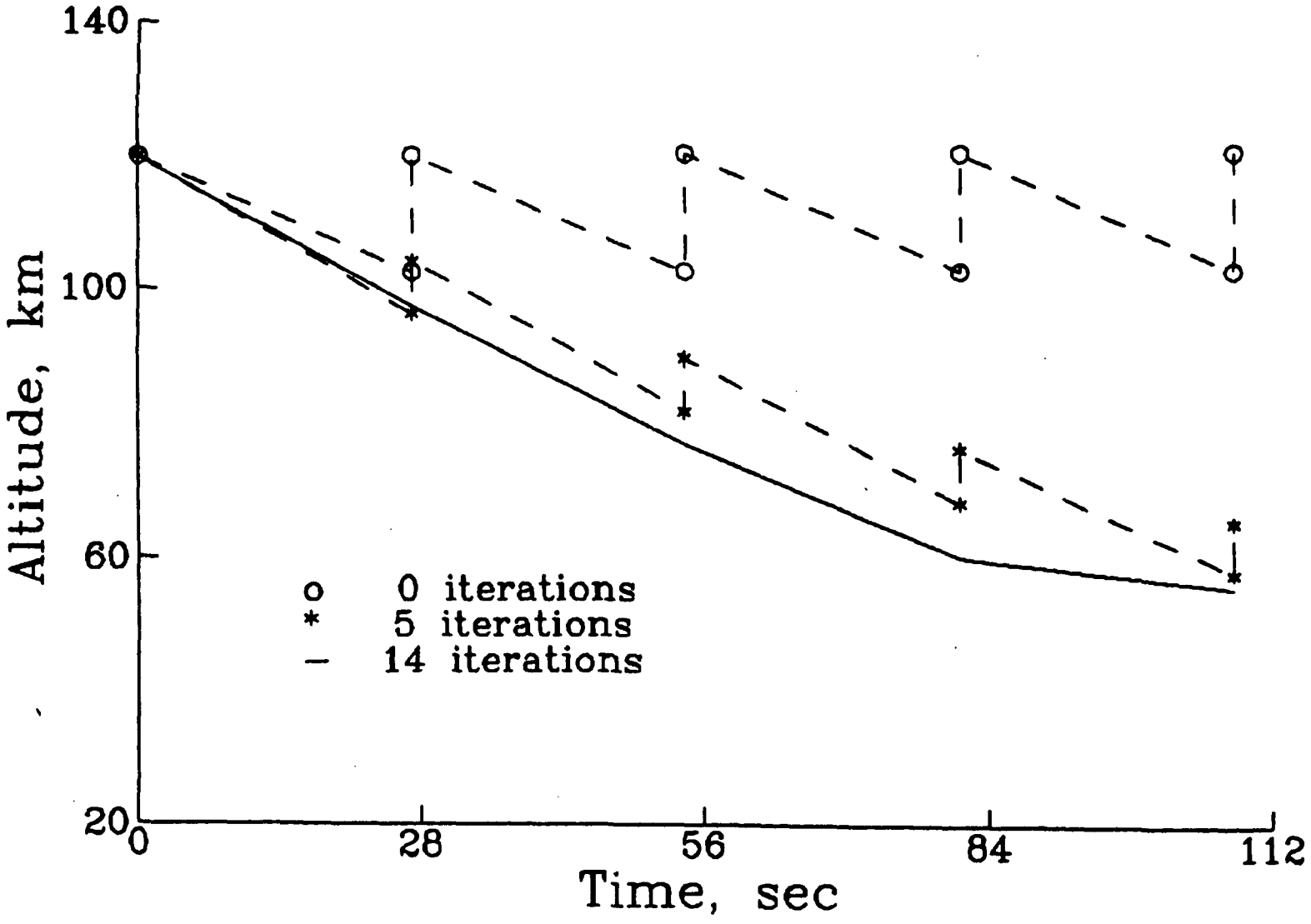

Fig.12 Successive approximations for altitude

FUEL-OPTIMAL TRAJECTORIES FOR AEROASSISTED NONCOPLANAR ORBITAL TRANSFER PROBLEM

Dr. D. S. Naidu
ODU Research Foundation
Norfolk, VA, 23508

ABSTRACT: The fuel-optimal control problem arising in noncoplanar orbital transfer employing aeroassist technology is addressed. The maneuver involves the transfer from high Earth orbit to low Earth orbit with plane change. A performance index is chosen to minimize the total fuel consumption for the transfer. Use of Pontryagin minimum principle leads us to a nonlinear, two-point, boundary value problem, which is solved by using a multiple shooting method.

NOMENCLATURE

A : constant = $S\rho_s/2m$

A_1 : constant = $C_{dO}S\rho_s H_a/2m$

A_2 : constant = $C_{LR}S\rho_s H_a/2m$

b : ratio of R_a/H_a

C_D : drag coefficient

C_{DO}: zero-lift drag coefficient

C_L : lift coefficient

C_{LR}: lift coefficient for maximum lift-to-drag ratio

c : ratio of C_L/C_{LR}

c : subscript for circularization or reorbit

D : drag force

d : subsript for deorbit

E_m : maximum of (L/D)

g : gravitational acceleration

g_s : gravitational acceleration at surface level

H : altitude

$\mathcal{H}$: Hamiltonian

J : performance index

K : induced drag factor

L : lift force

m : vehicle mass

R : distance from vehicle center of gravity to Earth center

R_a : radius of the atmospheric boundary

R_c : radius of the low Earth orbit

R_d : radius of the high Earth orbit

R_E : radius of Earth

R_s : distance from vehicle center of gravity to surface level

S : aerodynamic reference area

$_s$: subscript for surface level

t : time

V : velocity

v : normalized velocity

β : inverse atmospheric scale height

γ : flight path angle

ψ : heading angle

σ : bank angle

θ : down range angle or longitude

ϕ : cross range angle or latitude

δ : normalized density

λ : costate (Langrange) varible

μ : gravitational constant of Earth

ρ : density

τ : normalized time

ΔV : characteristic velocity

Δv : normalized characteristic velocity

1. INTRODUCTION

In space transportation system, the concept of aeroassisted orbital transfer opens new mission opportunities, especially with regard to the initiation of a permanant space station [1]. The use of aeroassisted maneuvers to affect a transfer from high Earth orbit (HEO) to low Earth orbit (LEO) has been reccommended to provide high performance leverage to future space transportation systems. The space-based, orbit transfer vehicle (OTV) is planned as a system for transporting payloads between LEO and other locations in space. The OTV, on its return journey from HEO, dissipates orbital energy through atmospheric drag to slow down to LEO velocity. In a synergetic maneuver for aeroassited, orbital transfer vehicles (AOTV's), the basic idea is to employ a hybrid combination of propulsive maneuvers in space and aerodynamic maneuvers in sensible atmosphere. Within the atmosphere, the trajectory control is achieved by means of lift and bank angle modulations Hence, this type of flight with a combination of propulsive and nonpropulsive maneuvers, is also called synergetic maneuver or space flight[2-7].

In this report, we address the fuel-optimal control problem arising in noncoplanar orbital transfer employing aeroassist technology. The maneuver involves the transfer from HEO to LEO with a presribed plane change and at the same time minimization of the fuel consumption. It is known that the change in velocity, also called the characteristic velocity, is a convenient parameter to measure the fuel consumption. For minimum-fuel maneuver, the objective is then to minimize the total characteristic velocity for deorbit, boost, and reorbit (or circularization). Use of Pontryagin minimum principle leads us to

a nonlinear, two-point, boundary value problem (TPBVP), which is solved by using a multiple shooting method [10-12].

2. BASIC EQUATIONS

The basic equations to be used are those for deorbit, aeroassist (or atmospheric flight), boost and reorbit (or circularization).

(i) Deorbit

Initially, the spacecraft is in cirualar orbit of radius R_d, well outside the Earth's atmosphere, moving with a circualar velocity $V_d = \sqrt{\mu/R_d}$. Deorbit is accomplished by means of an impulse ΔV_d, to transfer the vehicle from a circular orbit to elliptic orbit with perigee low enough to intersect the dense part of the atmosphere. Since the elliptic velocity at D is less than the circular velocity at D, the impulse ΔV_d is executed so as to oppose the circular velocity V_d. In otherwards, at point D, the velocity required to put the vehicle into elliptic orbit is less than the velocity required to maintain it in circular orbit. The deorbit impulse ΔV_d causes the vehicle to enter the atmosphere at radius R_a with a velocity V_e and flight path angle γ_e. It is known that the optimal-energy loss maneuver from the circular orbit is simply the Hohmann transfer and the impulse is parallel and opposite to the instantaneous velocity vector.

Using the principle of conservation of energy and angular momentum at the deorbit point D, and the atmospheric entry point E, we get [8],

$$V_e^2/2 - \mu/R_a = (V_d-\Delta V_d)^2/2 - \mu/R_d \tag{1}$$

$$R_a V_e \cos(-\gamma_e) = R_d(V_d-\Delta V_d) \tag{2}$$

from which solving for ΔV_d, we get

$$\Delta V_d = \sqrt{\mu/R_d} - \sqrt{2\mu(1/R_a-1/R_d)/\left[(R_d/R_a)^2/\cos^2\gamma_e-1\right]} \tag{3}$$

It is easily seen that the minimum value of the deorbit impulse ΔV_{dm} obtained at $\gamma_e = 0$, corresponds to an ideal transfer with the space vehicle grazing the atmospheric boundary. To ensure proper atmospheric entry, deorbit impulse ΔV_d must be higher than the mimimum deorbit impulse ΔV_{dm} which is given by

$$\Delta V_{dm} = \sqrt{\mu/R_d} - \sqrt{2\mu(1/R_a - 1/R_d)/[(R_d/R_a)^2 - 1]} \qquad (4)$$

(ii) Aeroassist

During the aeroassist (or atmospheric flight), the vehicle needs to be controlled by lift and bank angle to achieve the necessary velocity reduction (due to atmopheric drag) and the plane change.

Consider a vehicle with constant point mass m, moving about a nonrotating spherical planet. The atmosphere surrounding the planet is assumed to be at rest, and the central gravitational field obeys the usual inverse square law. The equations of motion for the vehicle are given by (Figure 1),

$$\frac{dH}{dt} = V\sin\gamma \qquad (5a)$$

$$\frac{dV}{dt} = -AC_D V^2 \exp(-H\beta) - (\mu/R^2)\sin\gamma \qquad (5b)$$

$$\frac{d\gamma}{dt} = AC_L V\cos\sigma\exp(-H\beta) + [V/R - \mu/(R^2V)]\cos\gamma \qquad (5c)$$

$$\frac{d\theta}{dt} = V\cos\gamma\cos\psi/(R\cos\phi) \qquad (5d)$$

$$\frac{d\phi}{dt} = (V/R)\cos\gamma\sin\psi \qquad (5e)$$

$$\frac{d\psi}{dt} = AC_L V\sin\sigma\exp(-H\beta)/\cos\gamma - (V/R)\cos\gamma\cos\psi\tan\phi \qquad (5f)$$

where $A = S\rho_s/2m$, $H = R - R_s$, $\rho = \rho_s \exp(-H\beta)$ and

$C_D = C_{DO} + KC_L^2$ for a drag polar.

Using the normalized variables,

$$\tau = t/\sqrt{R_a^3/\mu} \; ; \quad v = V/\sqrt{\mu/R_a} \qquad (6)$$

and the dimensionless constants,

$$h = H/H_a; \quad b = R_a/H_a; \quad \delta = \rho/\rho_s = \exp(-h\beta H_a) \qquad (7a)$$

$$c = C_L/C_{LR}; \quad C_{LR} = \sqrt{C_{DO}/K} \qquad (7b)$$

in (5), we get the normalized form as

$$\frac{dh}{d\tau} = bv\sin\gamma \tag{8a}$$

$$\frac{dv}{d\tau} = -A_1 b(1+c^2)\delta v^2 - \frac{b^2\sin\gamma}{(b-1+h)^2} \tag{8b}$$

$$\frac{d\gamma}{d\tau} = A_2 bc\delta v\cos\sigma + \frac{bv\cos\gamma}{(b-1+h)} - \frac{b^2\cos\gamma}{(b-1+h)^2 v} \tag{8c}$$

$$\frac{d\theta}{d\tau} = \frac{bv\cos\gamma\cos\psi}{(b-1+h)\cos\phi} \tag{8d}$$

$$\frac{d\phi}{d\tau} = \frac{bv\cos\gamma\sin\psi}{(b-1+h)} \tag{8e}$$

$$\frac{d\psi}{d\tau} = \frac{A_2 b\delta\lambda v\sin\sigma}{\cos\gamma} - \frac{bv\cos\gamma\cos\psi\tan\phi}{(b-1+h)} \tag{8f}$$

where, $A_1 = C_{DO}S\rho_s H_a/2m$; $A_2 = C_{LR}S\rho_s H_a/2m$

The plane change or orbit inclination, i, is related with cross range angle ϕ and heading angle ψ as [9]

$$\cos i = \cos\phi\cos\psi \qquad t_e \le t \le t_f \tag{9}$$

The orbit inclination changes through out the atmosphere segment and must have the required value at exit. For small values of cross range angle ϕ, i is given by the heading angle ψ itself.

(iii) Boost and Reorbit

During the atmospheric flight, the vehicle undergoes the plane change due to modulation in lift and bank angle. Because of the loss of energy during a turn, a second impulse is required to boost the vehicle back to orbital altitude.

The vehicle exits the atmosphere at point F, with a velocity V_f and flight path angle γ_f. The additional impulse ΔV_b, required at the exit point F for boosting into an elliptic orbit with apogee radius R_c and the reorbit (or circularization) impulse ΔV_c required to insert the vehicle into a circular orbit, are obtained by using the principle of conservation of energy and angular momentum at the exit point F, and the reorbit or circularization point C. Thus, we have,

$$(V_f+\Delta V_b)^2/2 - \mu/R_a = (V_c-\Delta V_c)^2/2 - \mu/R_c \tag{10}$$

$$(V_f+\Delta V_b)R_a\cos\gamma_f = R_c(V_c-\Delta V_c) \tag{11}$$

Solving for ΔV_b and ΔV_c from the above equations (10) and (11),

$$\Delta V_b = \sqrt{2\mu(1/R_a-1/R_c)/\left[1-(R_a/R_c)^2\cos^2\gamma_f\right]} - V_f \tag{12}$$

$$\Delta V_c = \sqrt{\mu/R_c} - \sqrt{2\mu(1/R_a-1/R_c)/\left[(R_c/R_a)^2/\cos^2\gamma_f-1\right]} \tag{13}$$

3. OPTIMAL CONTROL

It is known that the change in speed, ΔV, also called the characteristic velocity, is a convenient parameter to measure the fuel consumption. For minimum-fuel maneuver, the objective is then to minimize the total characteristic velocity. A convenient performance index is the sum of the characteristic velocities for deorbit, boost, and reorbit. Thus,

$$J = \Delta V_d + \Delta V_b + \Delta V_c \tag{14}$$

Where, ΔV_d, ΔV_b, and ΔV_c are the deorbit, boost, and reorbit characteristic velocities respectively, and are related as

$$\Delta V_d = \sqrt{\mu/R_d} - (R_a/R_d)V_e\cos(-\gamma_e) \tag{15}$$

$$\Delta V_c = \sqrt{\mu/R_c} - (R_a/R_c)(V_f+\Delta V_b)\cos\gamma_f \tag{16}$$

Alternatively, ΔV_d, ΔV_b and ΔV_c are also given by (3), (12), and (13) respectively. In the normalized form, the performance index becomes,

$$J = \Delta v = \Delta v_d + \Delta v_b + \Delta v_c \tag{17}$$

where,

$$\Delta v_d = \sqrt{1/a_d} - (v_e/a_d)\cos(-\gamma_e) \tag{18}$$

$$\Delta v_c = \sqrt{1/a_c} - \left[(v_f+\Delta v_b)/a_c\right]\cos\gamma_f \tag{19}$$

$$a_d = R_d/R_a; \quad a_c = R_c/R_a; \quad \Delta v = \Delta V/\sqrt{\mu/R_a} \tag{20}$$

Let us note that for a given circular orbit, the impulses ΔV_b and ΔV_c are completely determined by the state variables V_f and γ_f at the exit conditions of the atmospheric portion of the trajectory. The velocity V_e and the flight path angle γ_e at the entry point are dependent only on the magnitude of the deorbit impulse ΔV_d. Therefore, the optimal control problem needs to consider the segment of the trajectory within the atmosphere.

The first step in the optimization procedure using Pontryagin principle is to formulate Hamiltonian as [9]

$$\begin{aligned}\mathcal{H} = {} & \lambda_h bv\sin\gamma + \lambda_v\left\{-A_1 b(1+c^2)\delta v^2 - \frac{b^2\sin\gamma}{(b-1+h)^2}\right\} \\ & + \lambda_\gamma\left\{A_2 bc\delta v\cos\sigma + \frac{bv\cos\gamma}{(b-1+h)} - \frac{b^2\cos\gamma}{(b-1+h)^2 v}\right\} \\ & + \lambda_\phi\left\{\frac{bv\cos\gamma\sin\psi}{(b-1+h)}\right\} \\ & + \lambda_\psi\left\{\frac{A_2 b\delta\lambda v\sin\sigma}{\cos\gamma} - \frac{bv\cos\gamma\cos\psi\tan\phi}{(b-1+h)}\right\}\end{aligned} \tag{21}$$

where λ's are the costates corresponding to the states. The down range angle θ does not enter the right hand side of the equations of motion (5) and hence need not be considered for the optimization process.

The optimal control equations for lift and bank angle are given by

$$\frac{\partial\mathcal{H}}{\partial c} = 0; \quad \frac{\partial\mathcal{H}}{\partial\sigma} = 0 \tag{22}$$

leading to

$$c = C_{LR}\omega/C_{DO}2v\lambda_v; \quad \tan\sigma = \lambda_\psi/\lambda_\gamma\cos\gamma \tag{23}$$

where

$$\omega = \sqrt{\lambda_\gamma^2 + \left(\lambda_\psi/\cos\gamma\right)^2} \tag{24}$$

Realistically, the control C_L is bounded by the aerodynamic characteristics of the vehicle. Thus, for the constrained control,

$$|C_L| \leq C_{Lmax} \quad \text{or} \quad |c| \leq c_{max} \tag{25}$$

The costate (adjoint) equations are given by

$$\frac{d\lambda_h}{d\tau} = -\frac{\partial \mathcal{H}}{\partial h}; \qquad \frac{d\lambda_v}{d\tau} = -\frac{\partial \mathcal{H}}{\partial v}; \qquad \frac{d\lambda_\gamma}{d\tau} = -\frac{\partial \mathcal{H}}{\partial \gamma} \tag{26a}$$

$$\frac{d\lambda_\phi}{d\tau} = -\frac{d\mathcal{H}}{d\phi}; \qquad \frac{d\lambda_\psi}{d\tau} = \frac{d\mathcal{H}}{d\psi} \tag{26b}$$

Boundary Conditions

The initial and final boundary conditions are given for the normalized altitude h as

$$h(\tau=0) = 1.0, \quad h(\tau=\tau_f) = 1.0 \tag{27a}$$

and for the normalized velocity v, and the flight path angle γ as

$$(2-v_e^2)a_d^2 - 2a_d - v_e^2\cos^2\gamma_e = 0 \tag{27b}$$

$$\left[2-(v_f+\Delta v_b)^2\right]a_c^2 - 2a_c - (v_f+\Delta v_b)^2\cos^2\gamma_f = 0 \tag{27c}$$

The above relations are obtained using the principle of energy conservation and angular momentum conservation to the HEO-to-entry elliptic transfer orbit and the exit-to-LEO elliptic transfer orbit, respectively. The remaining boundary conditions are obtained from the transversality conditions on the costates. Thus, the optimization procedure, requiring the solution of the state equations (8) and the costate equations (26) along with the boundary conditions (27) leads us to the formulation of a nonlinear TPBVP, which is solved by using a multiple shooting method [10-12].

4. NUMERICAL DATA AND RESULTS

A typical set of numerical values used for simulation purposes is given below [3-6].

$C_{DO} = 0.1$; $K = 1.111$; $m/S = 300$ kg/m^2

$\rho_s = 1.225$ kg/m^3; $\mu = 3.986\times10^{14}$ m^3/sec^2

$\beta = 1/6900$ m^{-1}; $R_E = 6378$ KM

$H_a = 120$ KM; $R_d = 12996$ KM; $R_c = 6558$ KM

Using the above mentioned data, simulations are carried out. The optimal solution has the following entry and exit status.

Entry status: H_e = 120 KM; V_e = 9034.74 m/sec

γ_e = -4.435 degrees; ϕ_e = 0; ψ_e = 0

Exit status: H_f = 120 KM; V_f = 7009.29 m/sec

γ_f = -0.6217 deg; ϕ_f = 7.237 deg

ψ_f = 18.467 deg; total flight time = 500 sec

Characteristic velocities:

Deorbit characteristic velocity, ΔV_d = 1034.29 m/sec

Boost characteristic velocity, ΔV_b = 816.00 m/sec

Reorbit characteristic velocity, ΔV_c = 42.96 m/sec

Total characteristic velocity ΔV = 1893.25 m/sec

Time histories of altitude H, velocity V, and flight path angle γ, for total flight time of 540 seconds, are shown in Figure 2. Figure 3 shows lift C_L, bank angle σ, and lift-to-drag ratio L/D as a function of time from atmospheric entry to exit points. Those for the heating rate, dynamic pressure and density are shown in Figure 4.

Figure 2(a) shows the time history of altitude. The spacecraft enters and exits the atmosphere at an altitude of 120 KM. The minimum altitude reached is 46 KM. The velocity versus time is shown in Figure 2(b). The vehicle enters the atmosphere with a velocity of 9034.74 m/sec and leaves the atmosphere with a speed of 7009.29 m/sec, thus giving a velocity reduction of 2025.45 m/sec. The profile of flight path angle with time is shown in Figure 2(c). The spacecraft enters the atmosphere with an inclination of -4.435 degrees and exits with -0.6217 degrees. The conrol history is shown is shown in Figure 3(a). The vehicle enters the atmosphere with maximum lift capability and decreases slowly during the ramaining flight. Figure 3(b) shows the variation of bank angle during the atmospheric flight. Initially the vehicle enters the atmosphere with a bank angle of 154.75 degrees to pull the vehicle into the atmosphere but slowly drops to about 63.3 degrees and maitain at that value for the remainder of the flight.

The minimum-fuel transfer requires a total characteristic velocity of 1893.25 m/sec. It is of interest to compare this optimal aeroassisted transfer with the Hohmann transfer, which is maneuvered entirely in outer space, and has a deorbit characteristic velocity ΔV_{dh} of 1002.39 m/sec and the reorbit characteristic velocity ΔV_{ch} of 1192.25 m/sec, giving a total characteristic velocity for Hohmann transfer ΔV_h of 2194.64 m/sec. This shows that still the noncoplanar transfer with a plane change of 18.467 degrees is only 84 percent of the Hohmann (coplanar) transfer.

The heating rate Q_r, along the atmospheric trajectory, is computed for a sphere of radius of 1 meter, according to the relation [6],

$$Q_r = K_r \rho^{0.5} V^{3.08} \tag{28}$$

where, ρ is the atmospheric density in kg/km^3, V is the velocity in km/sec and K_r is the proportionality constant equal to 3.08×10^{-4}. Figure 4(a) shows the peak heating rate of 251.16 W/sq. cm. and the total integrated heating rate is found to be 21.0435 KW-sec/cm^2. As shown in Figure 4(b), the peak dynamic pressure is 103 KN/sq. m. The variation of density in Figure 4(c) ottained a peak value of 1.5367 kg/m^3.

Approximate Solutions

As a first cut in getting approximate solutions, we try to obtain the optimal solutions using the fact that the flight path angle γ is small. Using this approximation, the simulation has been repeated. Interestingly, it is found that we get almost the identical solutions with much less computation time. For example, in this case, the deorbit characteristic velocity ΔV_d is equal to 1034.29 m/sec, boost characteristic velocity ΔV_b is 816 m/sec and the reorbit characteristic velocity ΔV_c is found to be 43.01 m/sec, giving a total minimum characteristic velocity as 1893.3 m/sec. The total integrated heating rate is 21.0435 KW-sec/cm^2. The execution time on the computer is now only 41 percent of the execution time for the optimal solution without the approximation.

6. MULTIPLE SHOOTING METHOD

The determination of optimal control (23) requires the solution of a tenth order, nonlinear TPBVP consisting of state equations (8) and costate equations (26) and the associated boundary conditions (27). This can only be done by numerical methods. The multiple shooting method is one of the powerful methods for solving nonlinear TPBVP's. The corresponding OPTSOL code was developed by DFVLR establishment at Oberpfaffenhofen, West Germany [10-12].

In solving any boundary value problem with the given initial and final conditions, we asume additional initial data and integrate forward so that the solution satisfies the given final condition as well. This is also called a simple shooting method. Here, the convergence of the solution is highly sensitive to the assumed intial data. It is found that the error due to inaccurate initial data can be made arbitrarily small by performing the integration over sufficiently smaller subdivided panels within the given interval and thereby leading to the multiple shooting method. Thus, the multiple shooting method is a simultaneous application of the simple shooting method at several points within the interval of integration. Here, the trajectory may be restarted at intermediate points using new guesses. Jacobian matrices are formed for each segment. The resulting iteration scheme, based on

reducing all discontinuties at internal grid points to zero, leads to a system of linear algebraic equations.

Figure 5 shows the successive approximations of the altitude H, during the course of 0, 5, and 14 iterations. For the sake of clarity only 4 out of 20 intervals are shown. The initial guessed value for the altitude is 120 KM at every interval. It can be seen how the intitially large jumps at the subdivision points of the multiple shooting method are "flattened out" with the increase of iterations.

7. CONCLUSIONS

In this report, we have addressed the mimimization of fuel consumption during the atmospheric portion of an aeroassisted, noncoplanar, orbital transfer problem. The resulting two-point, boundary value problem was solved by using an efficient multiple shooting algorithm. The strategy for the atmospheric portion of the minimum-fuel transfer is to start initially with the maximum postive lift in order to recover from the downward plunge, and then to fly with a gradually decreasing lift such that the vehicle skips out of the atmosphere with a flight path angle near zero degrees. Also, initially, a bank angle greater than 90 degrees is used to pull the vehicle into the atmosphere, but is later reduced to produce the skip.

ACKNOWLEDGEMENTS

This research work was supported by a grant from NASA Langley Research Center, Hampton, under the technical monitorship of Dr Douglas B. Price, Assistant Head, Spacecraft Control Branch.

8 References

1. Walberg, G. D., "A survey of aeroassisted orbital transfer", J. Spacecraft, 22, 3-18, Jan.-Feb., 1985.

2. Vinh, N.-X., Optimal Trajectories in Atmospheric Flight, Elsevier Scietific Publishing Co., Amsterdam, 1981.

3. Dickmann, E. D., The effect of finite thrust and heating constraints on the synergetic plane change maneuver for space-shuttle orbiter-class vehicle, NASA TN D-7211, Oct. 1973.

4. Hull, D. G., Glitner, J. M., Speyer, J. L., and Maper, J., "Minimum energy loss guidance for aeroassisted orbital plane change", J. Guidance, Control, and Dynamics, 8, 487-493, July-Aug., 1985.

5. Vinh, N. X., and Hanson, J. M., "Optimal aeroassisted return from high Earth orbit with plane change", Acta Astronautica, 12, 11-25, 1985.

6. Miele, A., Baspur, V. K., and Lee, W. Y., "Optimal trajectories for aeroassisted noncoplanar orbital transfer", Acta Astronautica, 15, 399-412, June-July, 1987.

7. Mishne, D., and Speyer, J. L., "Optimal control of aeroassisted plane change maneuver using feedback expansions", Proc. AIAA Flight Mechanics Conf., Willimsburg, Aug., 1986.

8. Kaplan, M. H., Modern Spacecraft Dynamics and Control, John Wiley & Sons, New York, 1976.

9. Marec, J. P., Optimal Space Trajectories, Elsevier Scientific Publishing Comapany, Amsterdam, 1979.

10. H. B. Keller, Numerical Methods for Two-Point Boundary-Value Problems, Blaisdell Publ. Co., Waltham, 1968.

11. Stoer, J., and Bulirsch, R., Introduction to Numerical Analysis,, Springer-Verlag, New York, 1980.

12. Pesch, H. J., "Numerical computation of neighboring optimum feedback control schemes in real-time", Appl. Math. Optim., 5, 231-252, 1979.

****

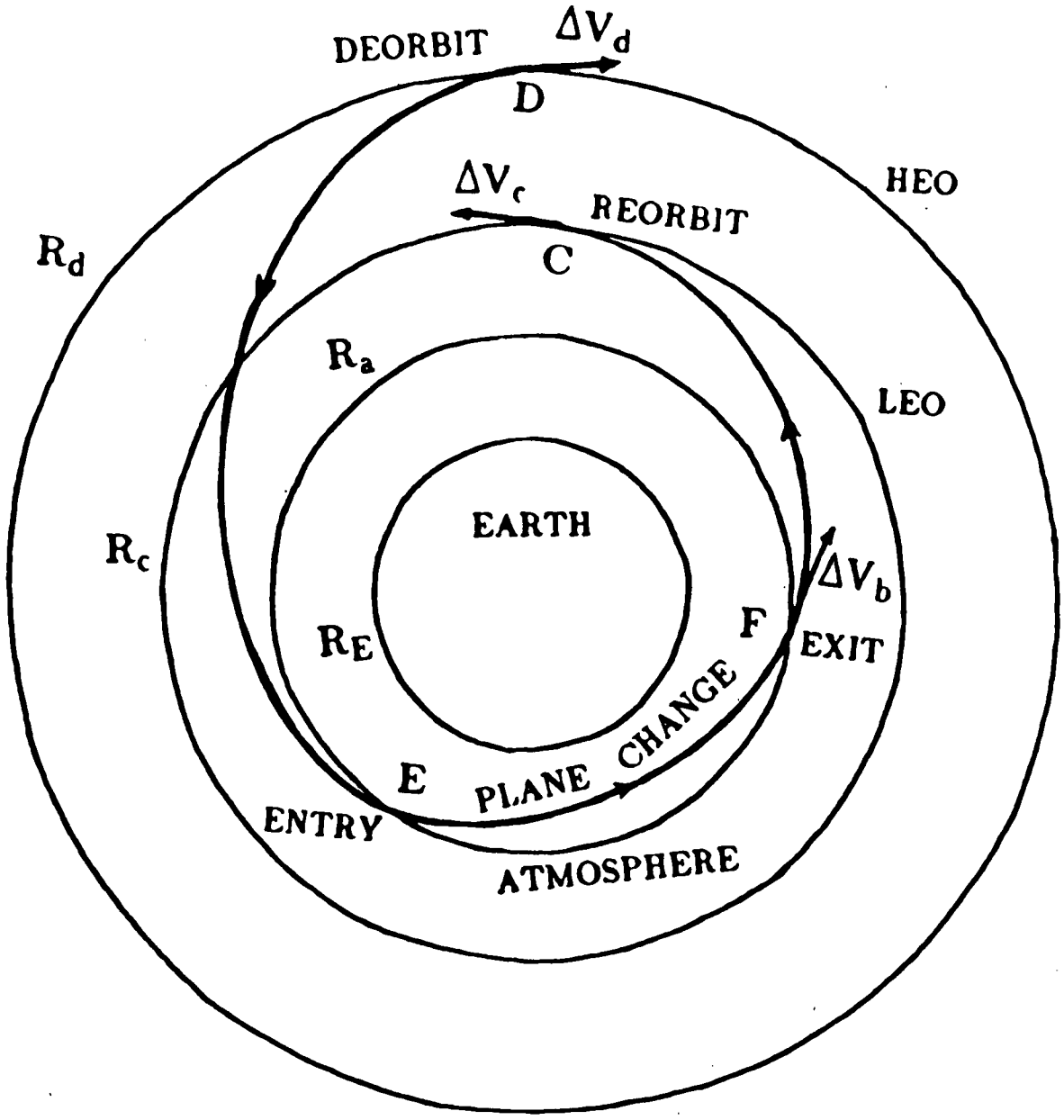

Fig. 1 Aeroassisted Orbital Plane Change

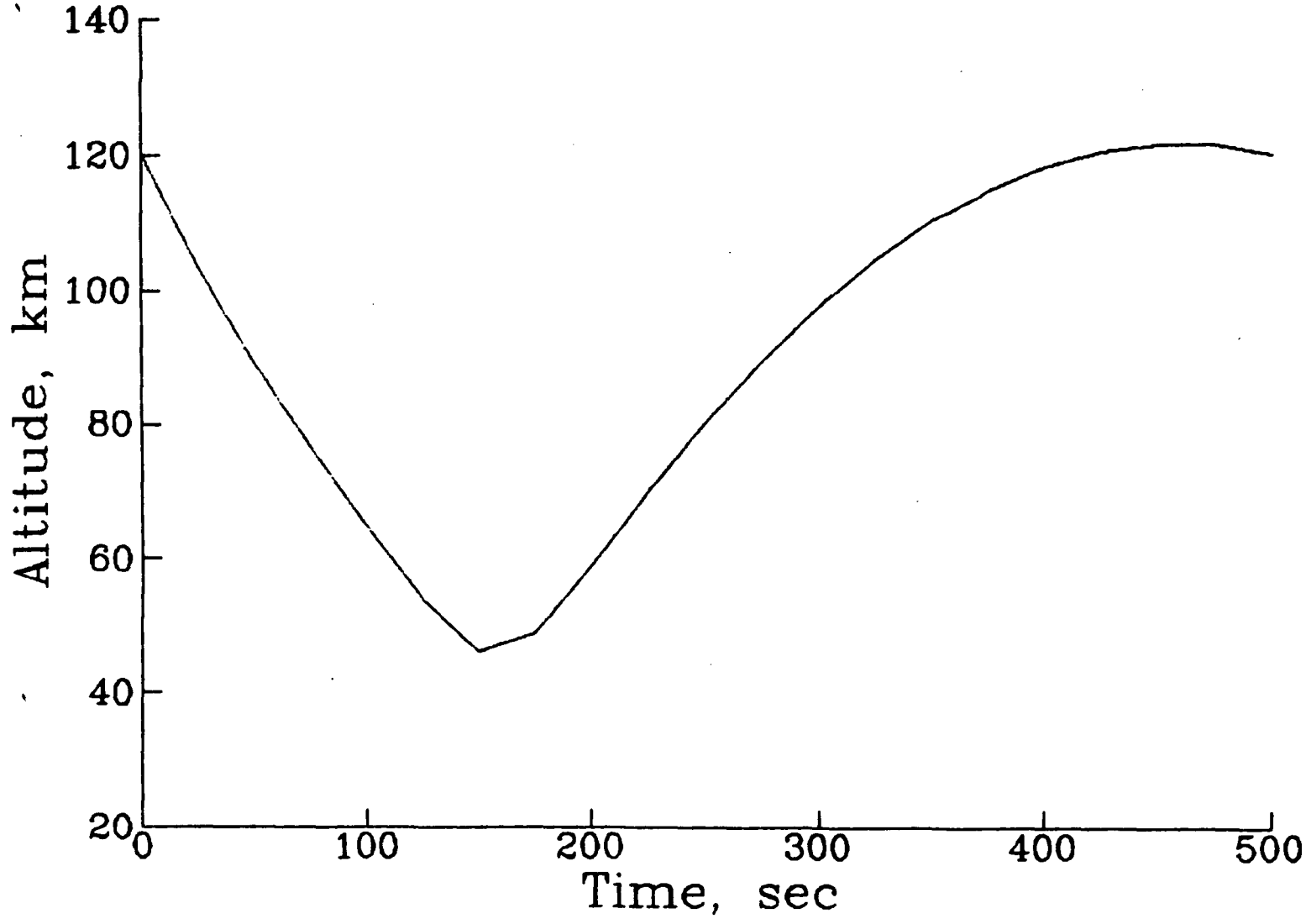

Fig.2(a) Time history of altitude

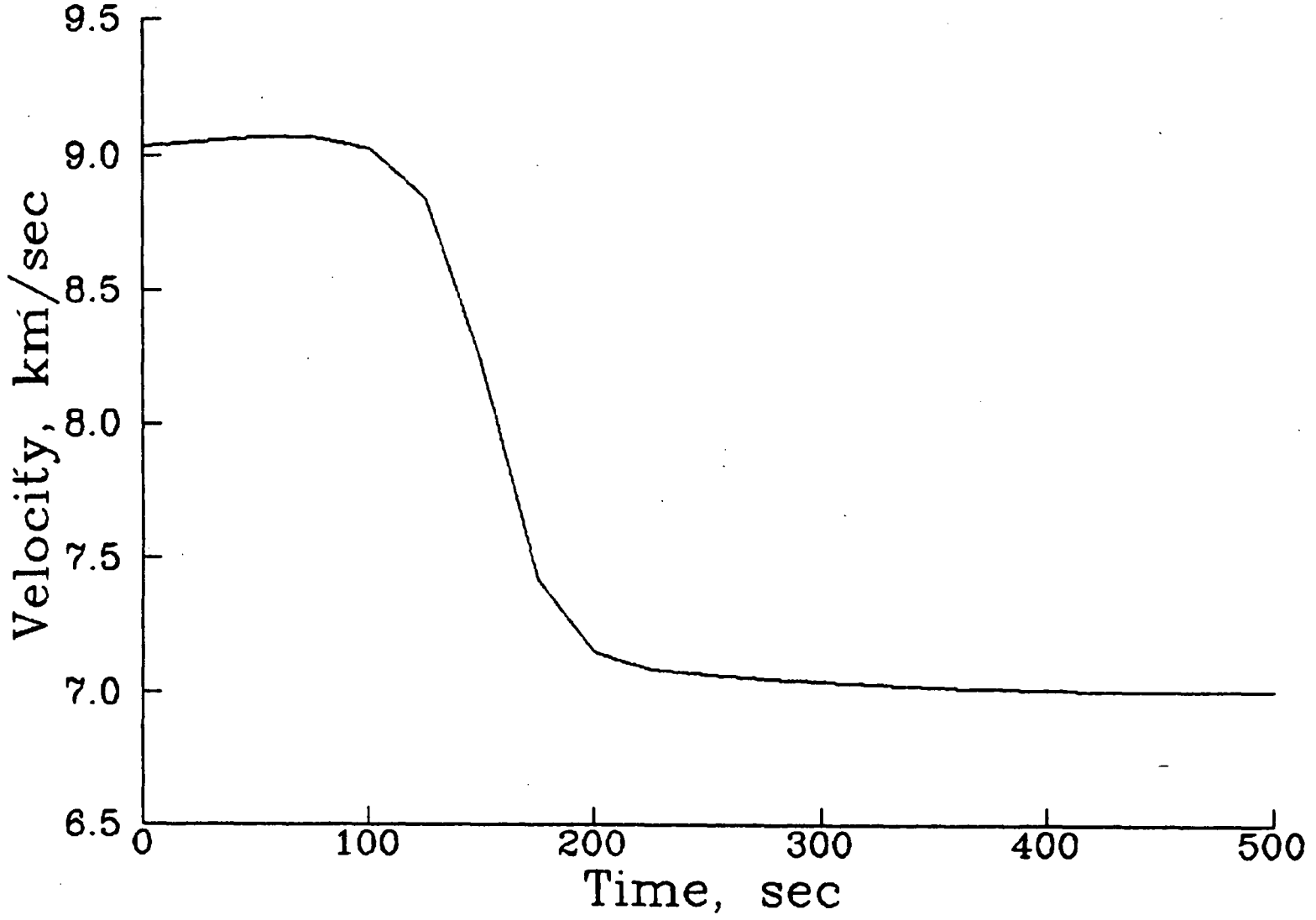

Fig.2(b) Time history of velocity

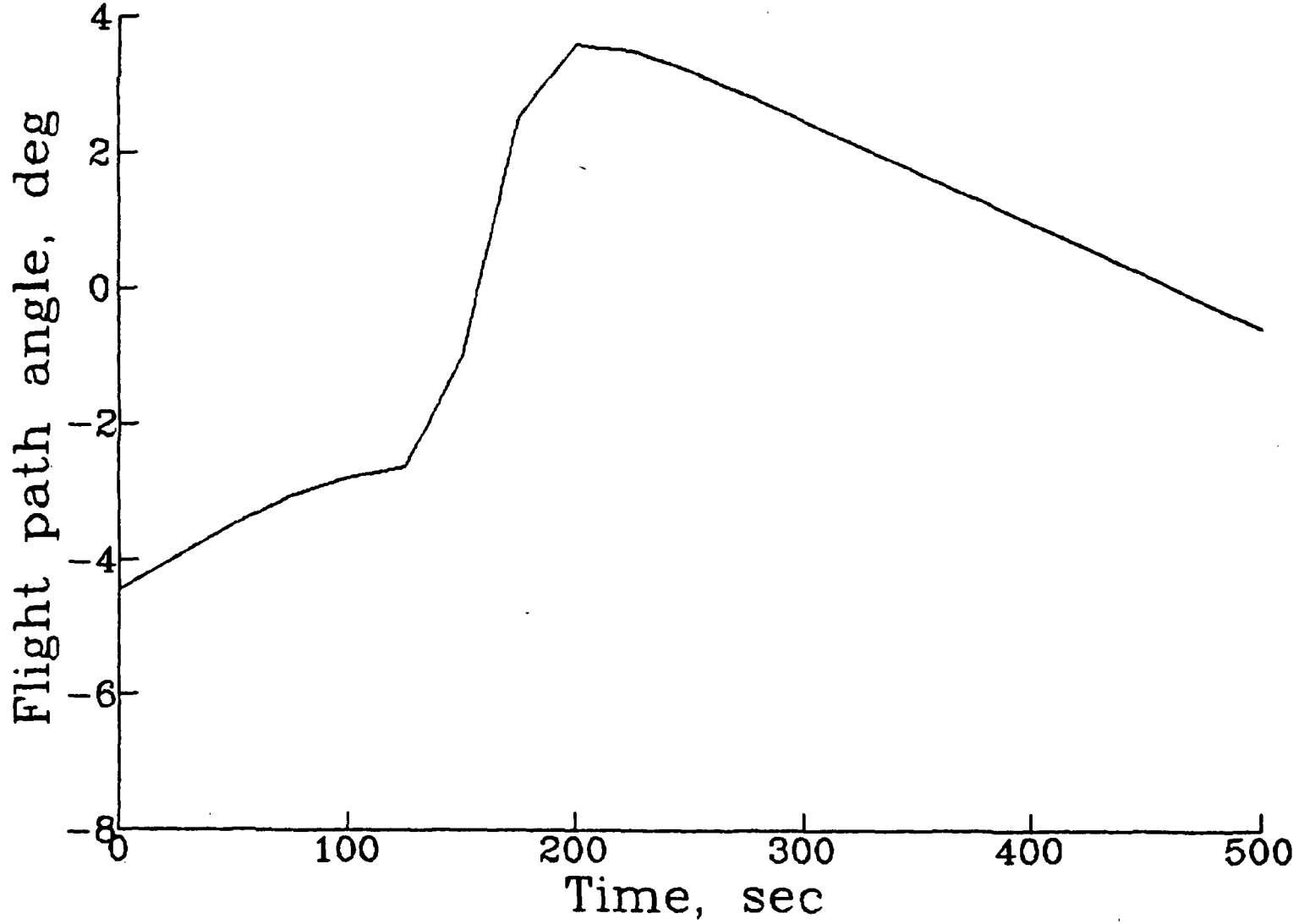

Fig.2(c) Time history of flight path angle

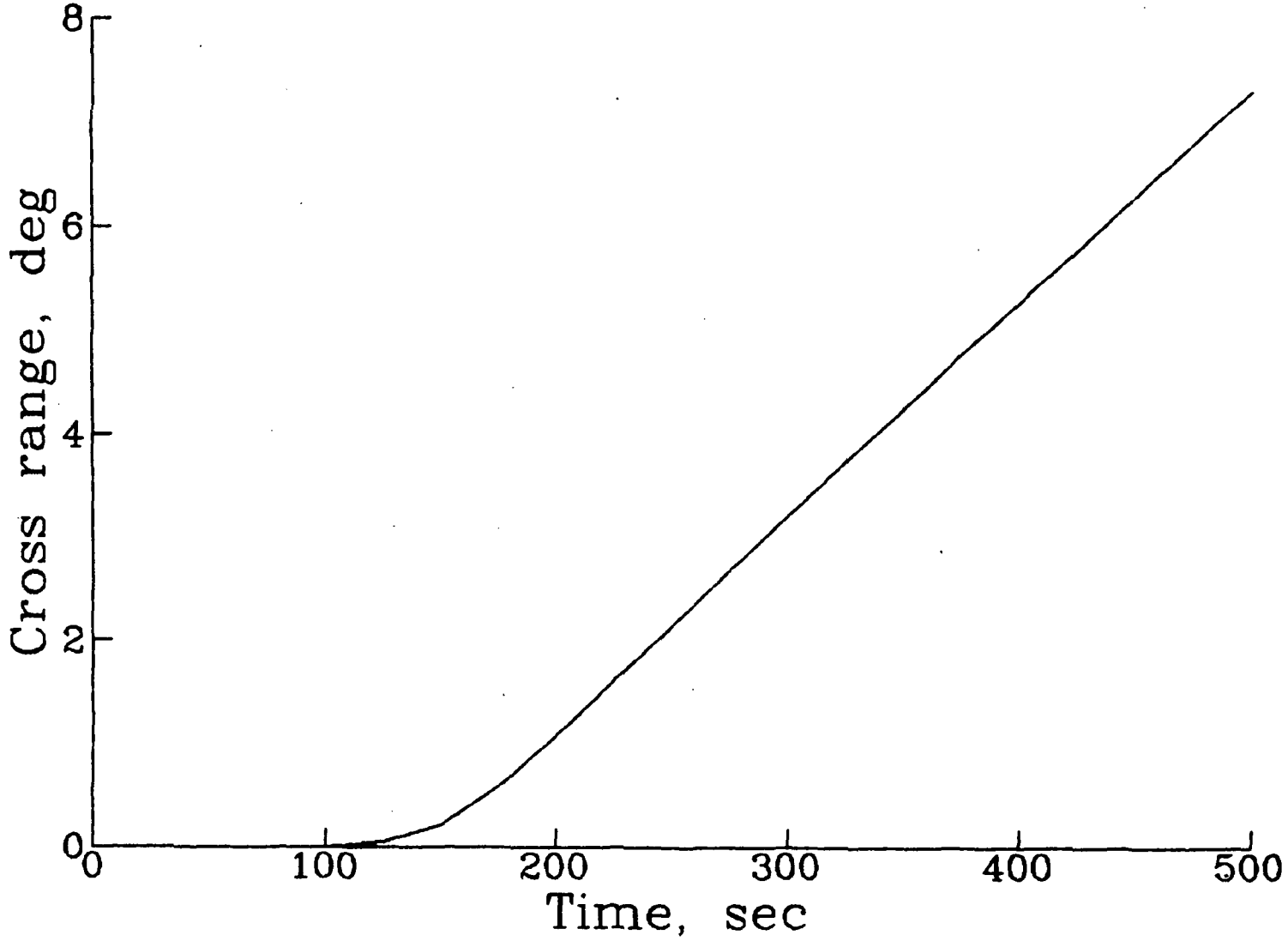

Fig.2(d) Time history of cross range

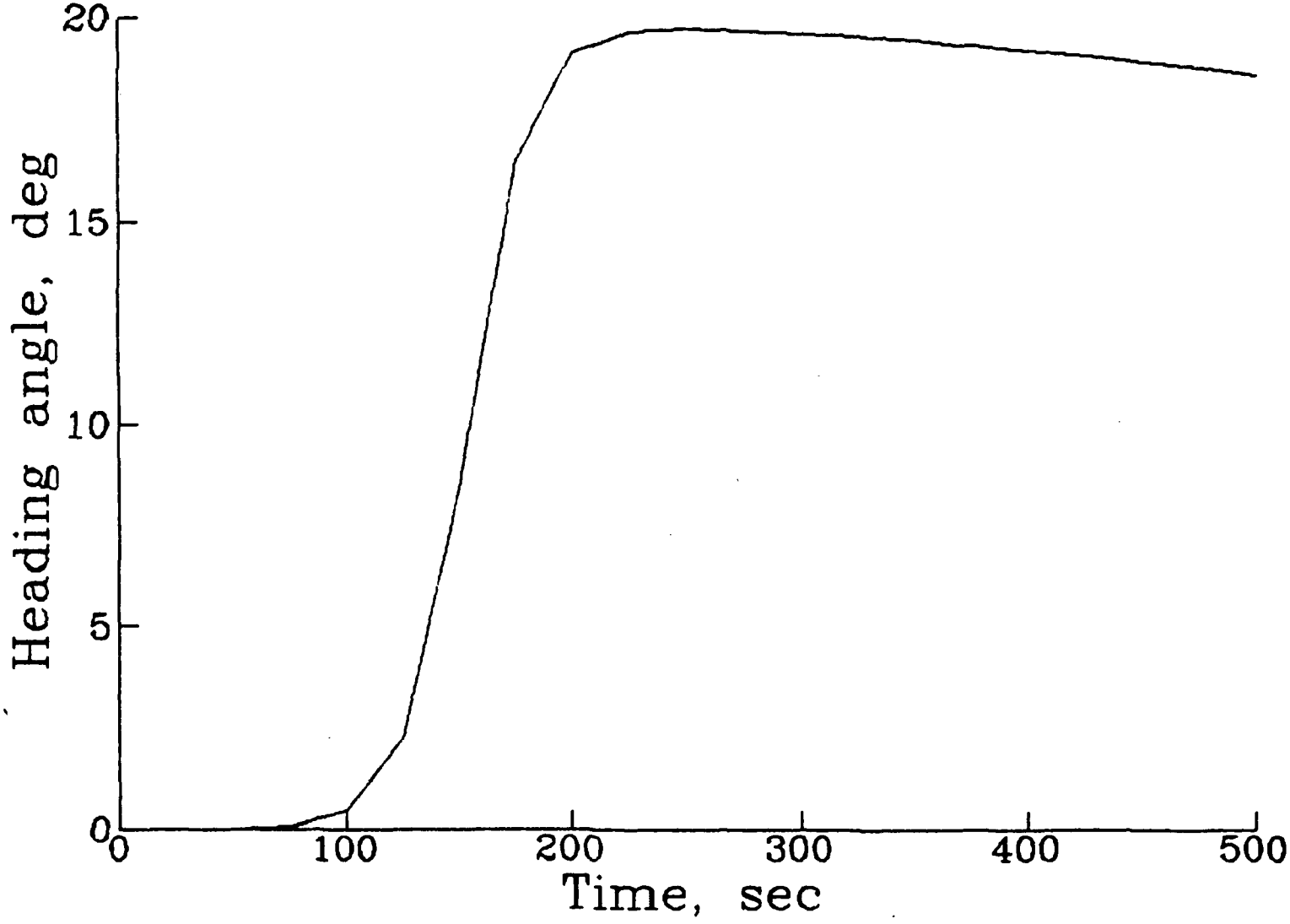

Fig.2(e) Time history of heading angle

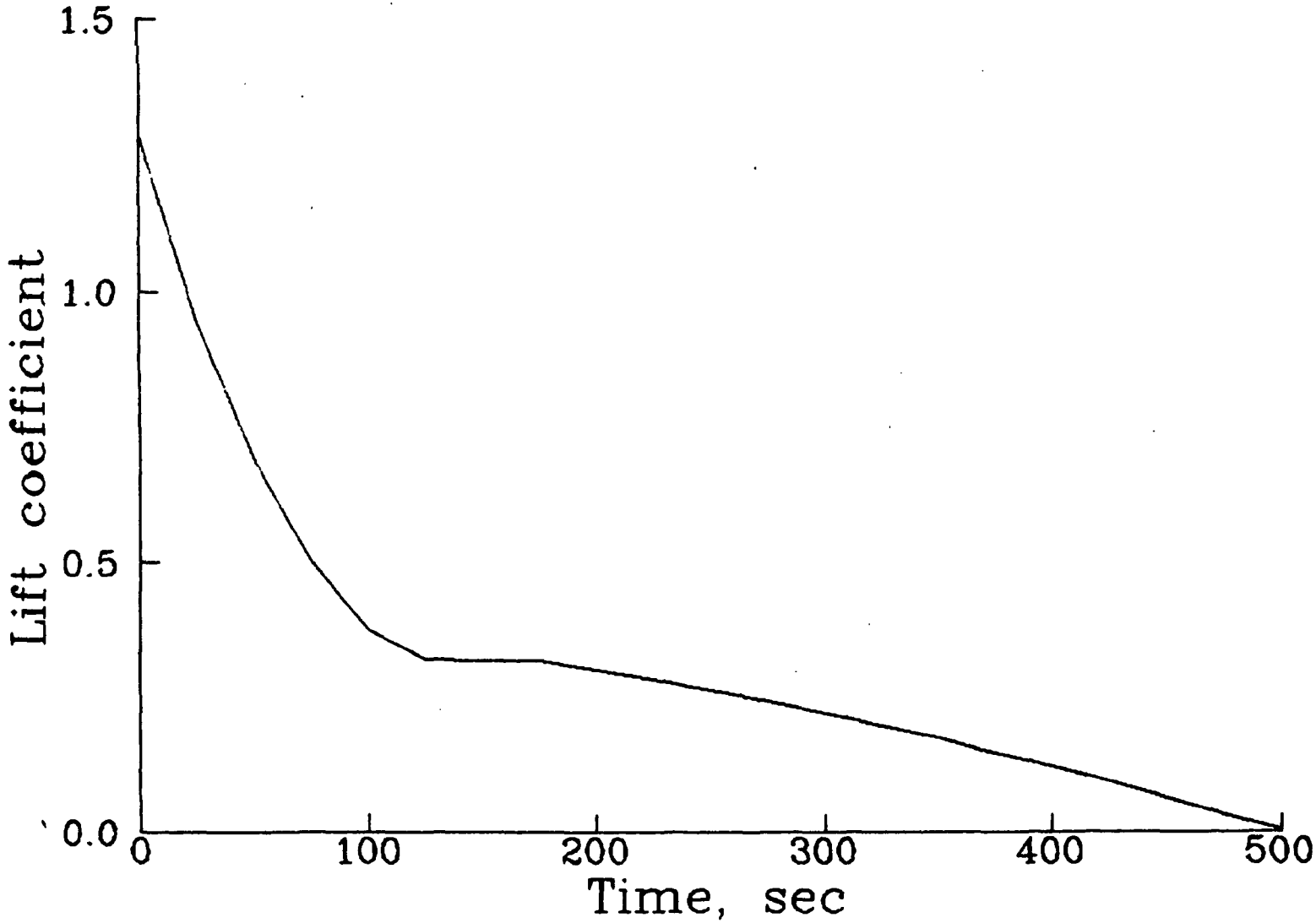

Fig.3(a) Time history of lift coefficient

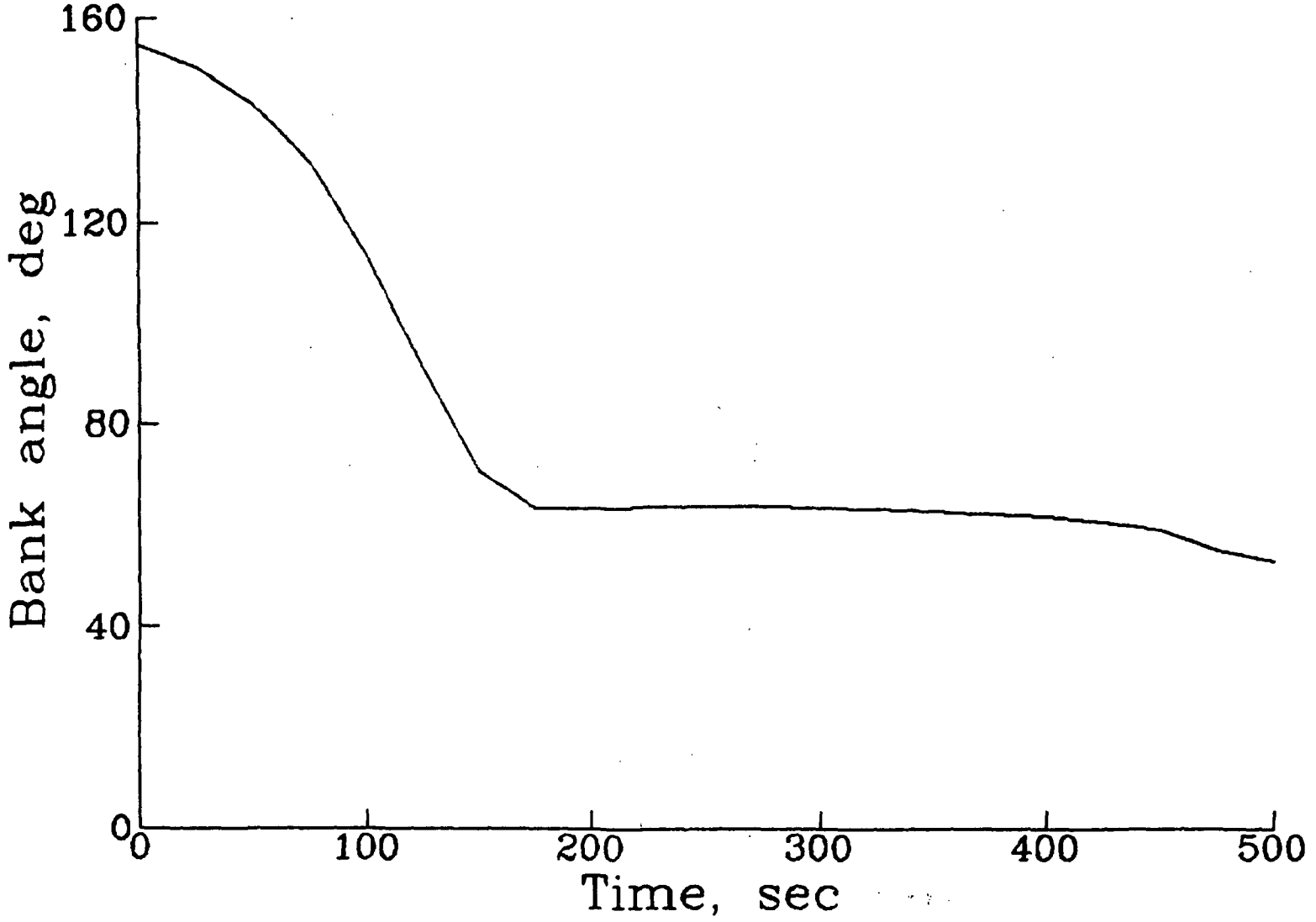

Fig.3(b) Time history of bank angle

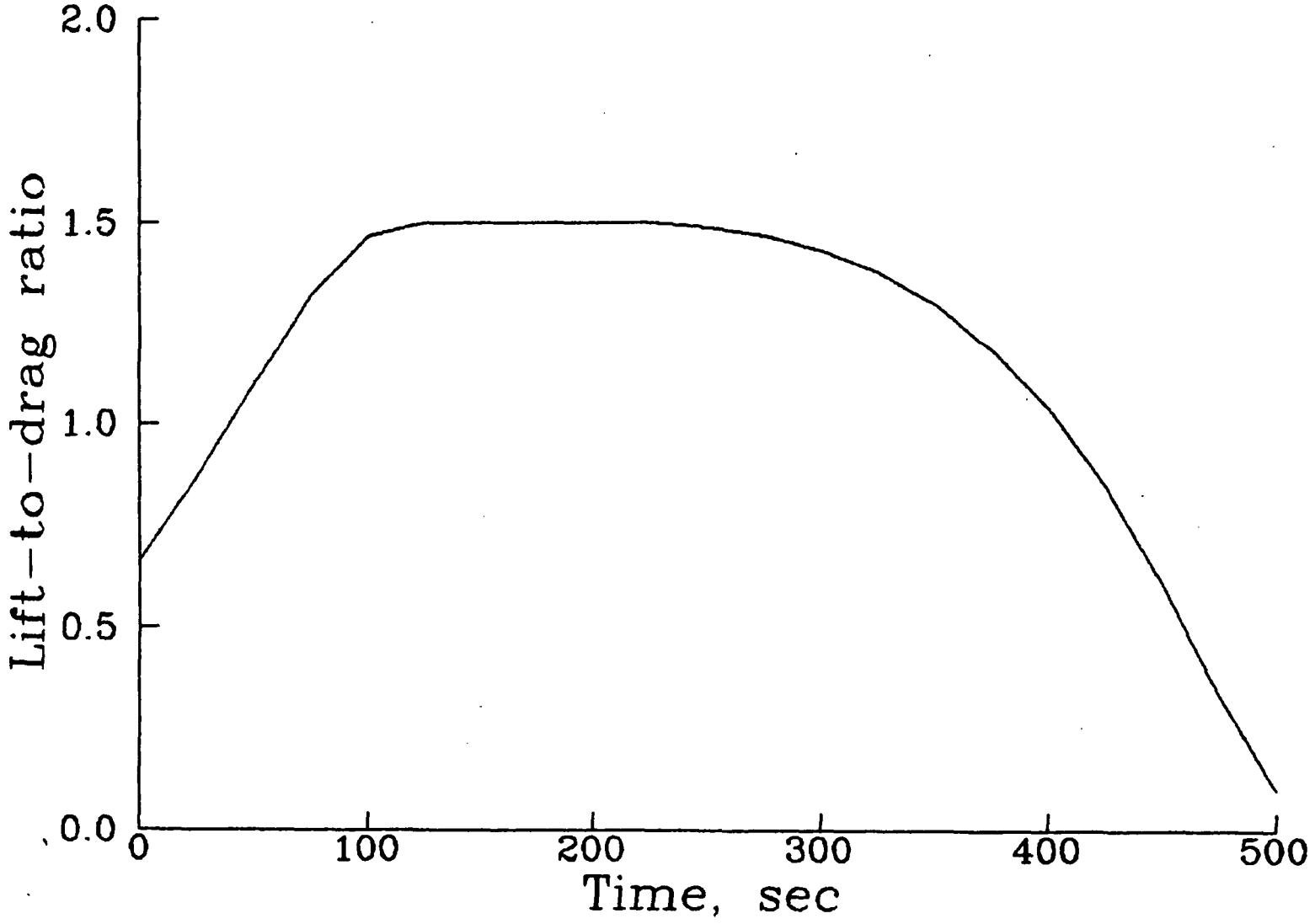

Fig.3(c) Time history of lift-to-drag ratio

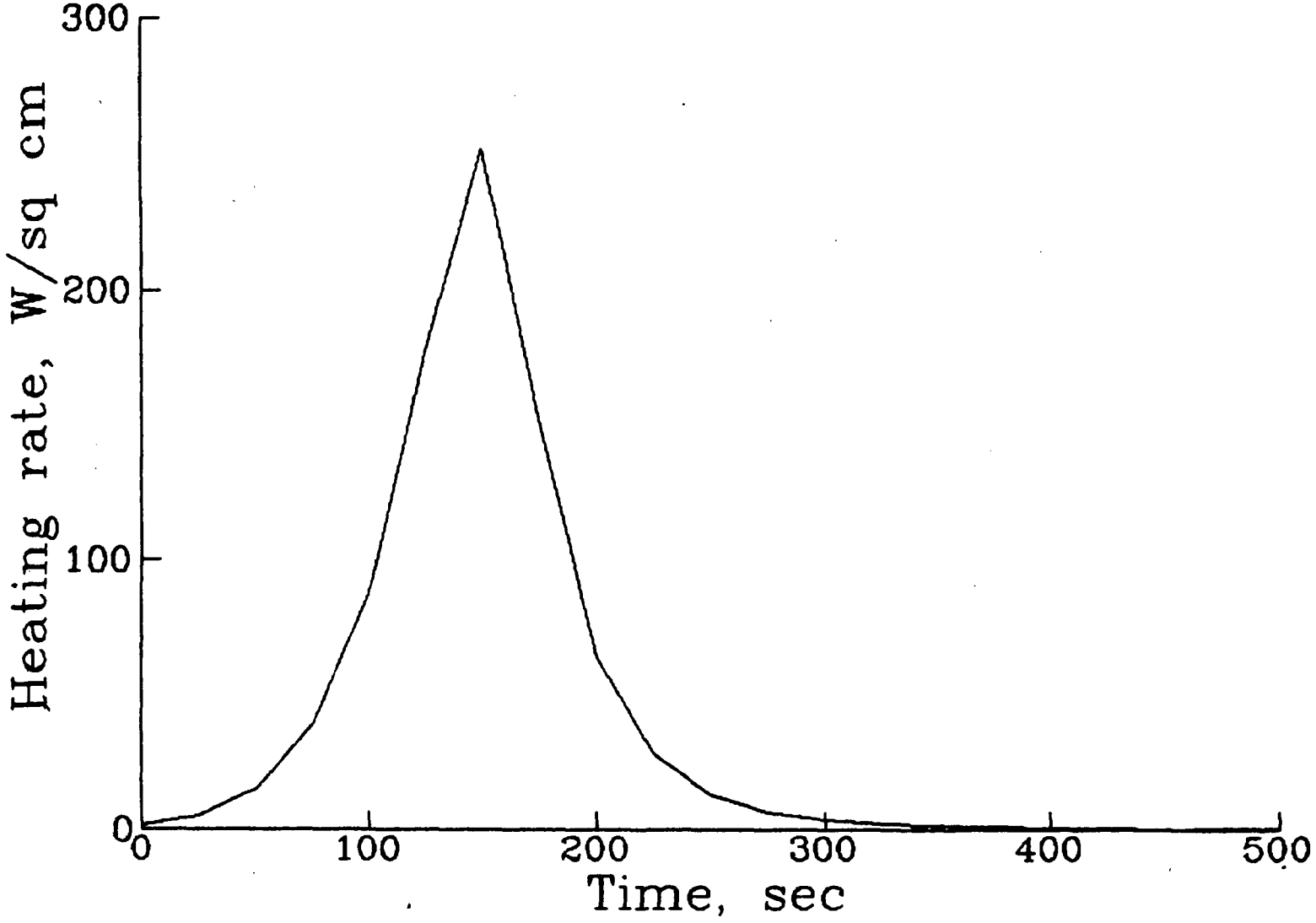

Fig.4(a) Time history of heating rate

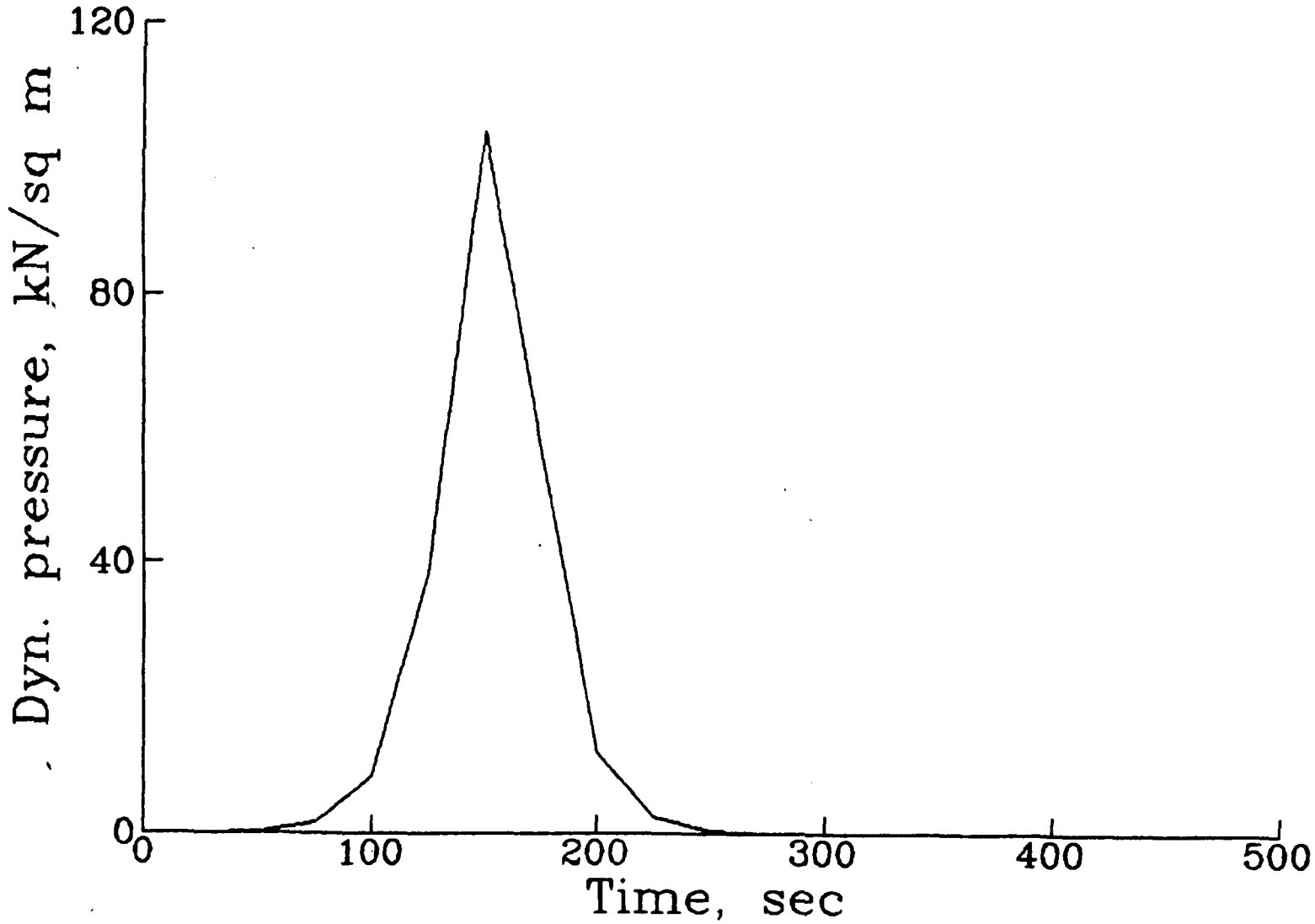

Fig.4(b) Time history of dynamic pressure

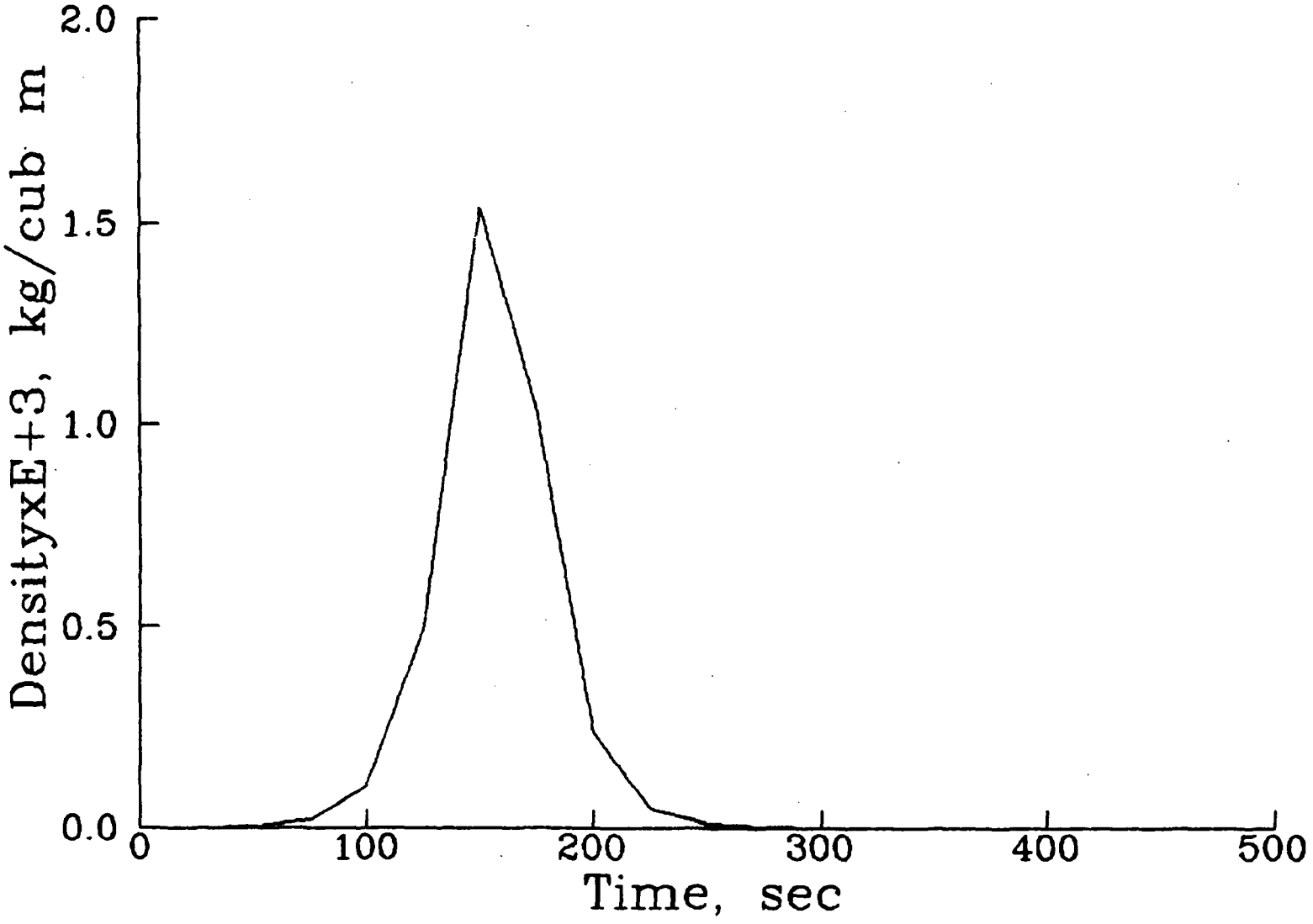

Fig.4(c) Time history of density

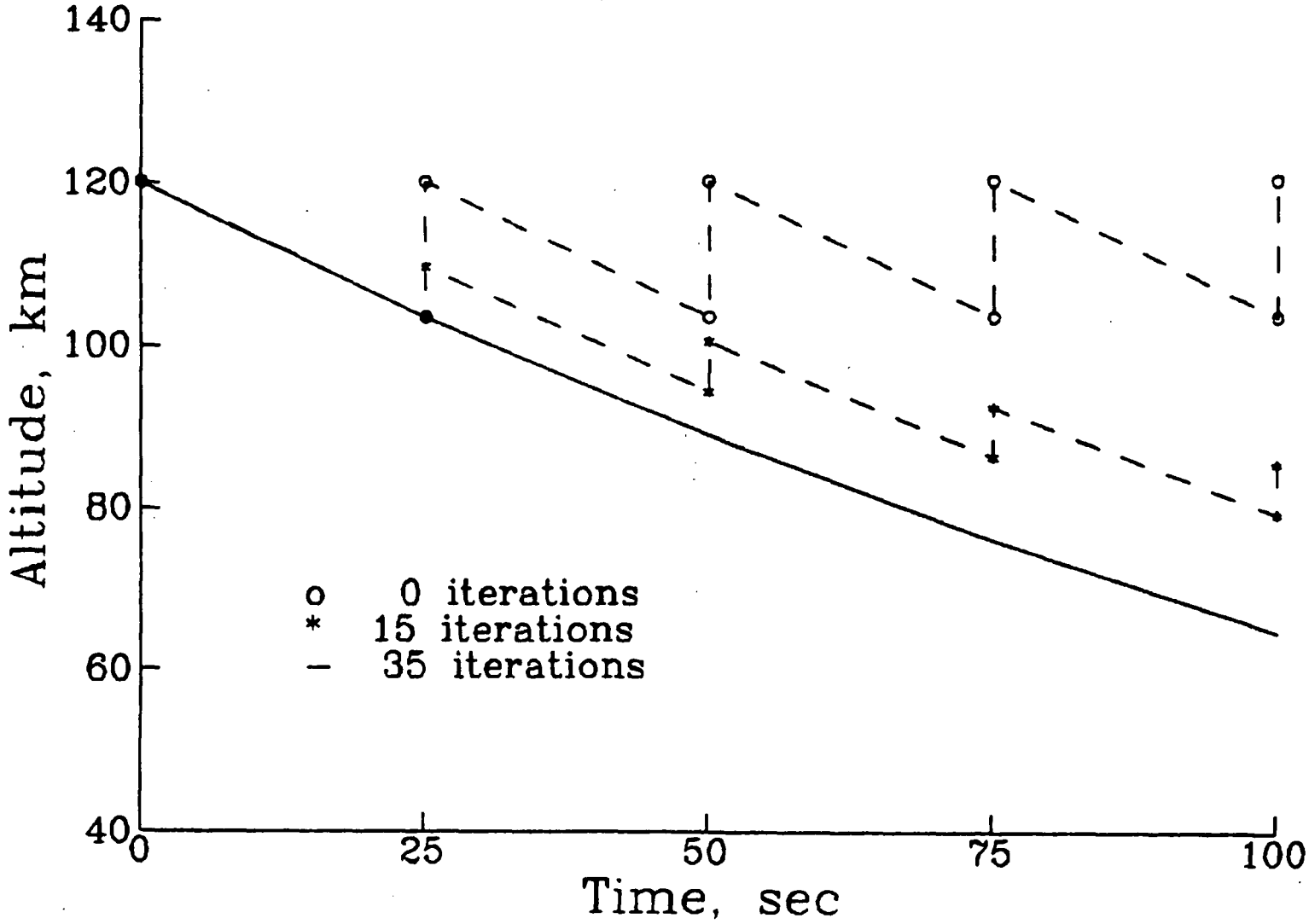

Fig.5 Successive approximations for altitude